Publications of the Astronomical Society of the Pacific, **127**:961–993, 2015 October

Observations of Solids in Protoplanetary Disks

Sean M. Andrews

Harvard–Smithsonian Center for Astrophysics, 60 Garden Street, Cambridge, MA 02138; sandrews@cfa.harvard.edu

Received 2015 May 29; accepted 2015 July 14; published 2015 September 28

ABSTRACT. This review addresses the state of research that employs astronomical (remote sensing) observations of solids ("dust") in young circumstellar disks to learn about planet formation. The intention is for it to serve as an accessible, introductory, pedagogical resource for junior scientists interested in the subject. After some historical background and a basic observational primer, the focus is shifted to the three fundamental topics that broadly define the field: (1) demographics—the relationships between disk properties and the characteristics of their environments and hosts; (2) structure—the spatial distribution of disk material and its associated physical conditions and composition; and (3) evolution—the signposts of key changes in disk properties, including the growth and migration of solids and the impact of dynamical interactions with young planetary systems. Based on the state-of-the-art results in these areas, suggestions are made for potentially fruitful lines of work in the near future.

Online material: color figures

1. MOTIVATION

The focus on origins, our cosmic context, is innate to astrophysics. The past two decades have seen remarkable progress and profound, renewed interest in the subject, primarily due to advances in the detection and characterization of planets around other stars (see Howard [2013] and Fischer et al. [2014] for recent reviews). There has been a considerable observational investment in studying exoplanet demographics, quantifying their diverse properties (masses, orbits; e.g., see the reviews by Marcy et al. 2005; Udry & Santos 2007; Winn & Fabrycky 2015) and identifying some fundamental trends (e.g., with metallicity or host mass; see Johnson et al. 2010). The return on that investment is a better understanding of the key processes that govern the formation and evolution of planetary systems. The observed properties of the exoplanet population place important boundary conditions on theoretical explanations of those processes.

The analogous study of the protoplanetary disks orbiting young stars offers a powerful complement to that work on exoplanets. Disk observations offer insights on the pivotal "initial conditions" available for making planetary systems, as well as the early coevolution and interaction of planets and their birth environments. Ultimately, the observed properties of both disks and exoplanets can be employed to inform, test, and refine models of the planet formation process (e.g., Benz et al. [2014] review a prominent approach to this problem).

The mutual evolution of disks and their planetary systems is terrifically complicated. The best theoretical models include functionally limited physics and do not yet successfully predict the measured properties of exoplanets, given the inferred parameters of disks. Much of the lingering uncertainty is due to our relative ignorance of disk properties. Disks are rich in information content for planet formation models, but observationally and physically messy. Fortunately, recent technical advances are facilitating new, improved disk observations that can drive rapid development in those models.

With that bright future in mind, this review is intended as an introductory pedagogical resource for the observational side of protoplanetary disk research. The targeted audience is junior members of the community (graduate students and postdoctoral scientists). The content is not comprehensive; the focus is primarily on fundamental issues and popular topics related to disk solids (referred to interchangeably as "dust" or "particles"). Although all the key techniques are represented, there is a bias toward measurements at radio wavelengths, motivated by the recent commissioning of the revolutionary Atacama Large Millimeter/submillimeter Array (ALMA).

The review is organized as follows: § 2 offers a brief historical overview of disk observations, to provide some context for the ongoing work in the field. § 3 is a primer for interpreting observations of disk solids. § 4, 5, and 6 discuss the state of the art constraints on the demographics of the disk population, the inferred structures and physical conditions in disks, and insights on how those properties change with time, respectively. § 7 summarizes some open questions, with an eye toward future observational research.

2. HISTORICAL BACKGROUND

There is a long history of theoretical interest in protoplanetary disks, particularly the precursor to the solar system (the

solar nebula). Although there are earlier metaphysical conceptions, the familiar "nebular hypothesis" of a flattened, rotating structure as the origin of the observed coplanar planetary orbits was well formulated by Kant (1755) and Laplace (1796) before subsequent elaboration shifted to astronomers (e.g., Moulton 1900, 1905; Chamberlin 1900; see the historical reviews by Brush [1978a, 1978b, 1981] or Wood & Morfill [1988]). As more physically motivated theories of the star formation process were developed, such a disk structure was found to be a natural consequence of gravitational collapse in a molecular cloud core endowed with some angular momentum (Hoyle 1960; Cameron 1962; Cassen & Moosman 1981; Cassen & Summers 1983; Terebey et al. 1984).

Meanwhile, taking the existence of such disks as given, the theoretical study of their physical characteristics and evolution was split into two camps; one focused on planet formation (see the classic reviews by Cameron [1988] and Lissauer [1993], or the historical summary of a seminal period by Brush [1990]), and the other emphasized the processes of accretion and momentum transport (see Pringle 1981; Papaloizou & Lin 1995). These topics were mature enough to accumulate a vast literature by the 1980s, well before many astronomers were completely satisfied with the observational evidence for such disks (let alone extrasolar planetary systems).

The discovery and early characterization of young stars, the T Tauri (or Orion) variables (Joy 1945, 1949; Herbig 1962) and their massive Herbig AeBe counterparts (Herbig 1960), hinted at a close connection with circumstellar material. Influenced by the star formation simulations of Larson (1969, 1972), the blue excesses, line emission (e.g., Strom et al. 1971, 1972), and enhanced infrared continua (Mendoza 1966, 1968; Geisel 1970; Gillett & Stein 1971) associated with these young stars were seen as evidence for the circumstellar "shells" or envelopes predicted to be remnants of the cloud collapse. There was debate on whether these features were produced solely by hot ($\sim 10^4$ K) gas (e.g., Strom et al. 1971, 1972, 1975; Strom 1972; Rydgren et al. 1976; Warner et al. 1977), or if cooler ($\sim 10^2$ K) dust was an important contributor (e.g., Cohen 1973, 1980; Cohen & Kuhi 1979; Rydgren & Vrba 1981, 1983; Rydgren et al. 1982). Ultimately, it was recognized that both components are required; an emerging model attributed the hot (blue) excess to accretion shocks at the stellar surface (Lynden-Bell & Pringle 1974; Uchida & Shibata 1984; Bertout et al. 1988) and the cool (red) excess to dust on approximately AU scales (Cohen 1983; Cohen et al. 1985; Lada & Wilking 1984; Rydgren 1984; Rydgren & Zak 1987).

That realization was part of a pronounced shift in the mid-1980s away from "shells" and toward accretion disks. Rather than being precipitated by a single measurement or study, this conceptual evolution was driven by the confluence of several key independent lines of indirect evidence (most of these were clearly summarized in the seminal review by Shu et al. [1987]): the observed large (linear) polarizations of T Tauri stars were indicative of scattering off of flattened dust structures (e.g., Elsasser & Staude 1978; Vrba et al. 1979; Bastien 1982; Bastien & Menard 1988), which were just then being resolved in the near-infrared (Grasdalen et al. 1984; Beckwith et al. 1984; Strom et al. 1985); collimated bipolar outflows were being linked to an accretion disk origin (e.g., see the review by Lada [1985]); asymmetric (blueshifted) forbidden emission line profiles were interpreted as smaller scale winds or outflows that are partially obscured by an extended disk (e.g., Edwards et al. 1987; Cabrit et al. 1990); the outburst behavior in the FU Orionis variables was being associated with disk instabilities (Hartmann & Kenyon 1985; Lin & Papaloizou 1985), forging important links to the fields of cataclysmic variables (e.g., Kenyon & Webbink 1984; Lin et al. 1985) and viscous accretion disks (e.g., Lynden-Bell & Pringle 1974); optically thin millimeter/radio flux measurements confirmed that spherical dust distributions were inconsistent with the observed optical extinctions (Beckwith et al. 1990; see also Churchwell et al. 1987); and perhaps most influentially, increased access to infrared measurements, especially from *IRAS* (e.g., Rucinski 1985; Strom et al. 1988; Harris et al. 1988; Wilking et al. 1989), was motivating substantial modeling developments to explain the broadband spectral energy distributions (SEDs) in the context of irradiated dust disks (Adams & Shu 1986, Adams et al. 1987, 1988; Kenyon & Hartmann 1987).

In the minds of many researchers in the field, this shift in thinking culminated in a spectacular "seeing is believing" confirmation with resolved *Hubble Space Telescope* (*HST*) observations of disks in silhouette against the bright background of the Orion Nebula (O'dell et al. 1993; O'dell & Wen 1994; McCaughrean & O'dell 1996); a favorite example is shown in Figure 1. Around the same time, spatially resolved images of scattered light from *HST* (e.g., Burrows et al. 1996; Stapelfeldt et al. 1998) and thermal emission from the first generation of millimeter-wavelength interferometers (e.g., Sargent & Beckwith 1987, 1991; Koerner et al. 1993; Hayashi et al. 1993; Lay et al. 1994, 1997; Koerner et al. 1995; Dutrey et al. 1994, 1996; Mundy et al. 1996; Mannings & Sargent 1997) also played key roles in shaping the field.

Since then, the past $\sim$20 years have seen a remarkable proliferation of disk measurements that have nurtured the growth of a new, observational branch to the study of planet formation. It is not unreasonable to say that unresolved photometry and spectroscopy from the *Spitzer Space Telescope* accounts for a substantial share of the maturation of this field, in terms of demographics, dust composition and basic structure, rapid development of radiative transfer tools, and hints of evolution (e.g., Hillenbrand et al. 2008; Evans et al. 2009; Furlan et al. 2009, 2011). But meanwhile, spatially resolved data have been playing a steadily increasing role in those advances. With ambitious new technologies being commissioned, spatially resolved observations are poised to facilitate transformational progress.

FIG. 1.—Optical *HST* image of a nearly edge-on disk, seen in silhouette against the bright background emission of the Orion Nebula (Robberto et al. 2013). It was direct images like this that ultimately confirmed the theoretical ideas about the ubiquity and basic structures of disks around young stars. *Image credit: NASA, ESA, M. Robberto (STScI/ESA), and the Hubble Space Telescope Orion Treasury Project Team.* See the electronic edition of the *PASP* for a color version of this figure.

3. ESSENTIALS OF DISK OBSERVATIONS

Before delving into the state of the field and its potential future directions, it will be useful to go through a basic primer on disk observations and how they are interpreted in the context of disk properties.

Protoplanetary disks are dense, geometrically flattened circumstellar structures composed of a trace population of solids (initially ~1% by mass) suspended in a reservoir of (primarily) molecular gas. Gravity and angular momentum conservation ensure that disk densities decrease with radial separation from the host star, r (e.g., Terebey et al. 1984; Lynden-Bell & Pringle 1974); thermal pressure and turbulence determine how the densities fall off with height above the midplane, z (e.g., Whipple 1972; Weidenschilling 1977a; Dubrulle et al. 1995). The disk temperatures are almost entirely controlled by the passive stellar irradiation of the solids (Adams et al. 1987; Kenyon & Hartmann 1987), which have large broadband opacities that dominate the heating and cooling rates (Ossenkopf & Henning 1994; Pollack et al. 1994). Irradiation heating implies that temperatures decrease with r. Starlight intercepted by dust in the disk surface layers (atmosphere) is reradiated out to space and deeper into the disk structure; this results in a vertical thermal inversion, where the midplane is cooler than the atmosphere (Calvet et al. 1991; Chiang & Goldreich 1997; D'Alessio et al. 1998). In this basic structural framework (see § 5 for more details), the solids completely dominate the opacity budget. Coupling this with the high sensitivity of broadband detectors, it makes sense that observations of the continuum emission generated by solids are the most efficient probes of many disk properties.

That continuum has two primary contributors, from thermal (reprocessed stellar energy, which dominates) and scattered (reflected starlight) radiation. The specific intensity at frequency ν along a given line of sight s is intimately related to the physical conditions, structural distribution, and material properties of the disk solids through the formal radiative transfer equation,

$$dI_\nu = \rho\kappa_\nu(S_\nu - I_\nu)ds, \tag{1}$$

where ρ is the density, κ_ν is the (absorption + scattering) opacity per gram of the solid material, and S_ν is the source function (the ratio of emissivity to opacity, with absorption and scattering contributions). The condensed notation of equation (1) obscures the tremendous complexity of the radiative transfer problem. A complete solution requires the energy input from the host star as well as the three-dimensional distributions of ρ, κ_ν (and the associated directional scattering properties), and S_ν. The major challenge is that S_ν also depends on these properties (ρ, κ_ν, etc.). In practice, this complicated feedback is handled numerically, often with Monte Carlo simulations (Lucy 1999; Bjorkman & Wood 2001) that treat the propagation of photons into the disk, the corresponding heating of the solids, and the escape of photons to the observer (e.g., Wolf et al. 1999; Whitney et al. 2003; Dullemond & Dominik 2004a; Robitaille et al. 2006; Pinte et al. 2006; Min et al. 2009; Robitaille 2011).[1]

3.1. Thermal Emission

Although appreciating the intrinsic complexity of radiative transfer in disks is valuable, it offers little intuition for interpreting the data. But with some simplifications, a more pedagogical model that captures the essential features of the thermal emission can be constructed. Consider a disk where scattering is negligible, the structure is vertically thin ($S_\nu\sim$ constant along s), and the material is in thermodynamic equilibrium [$S_\nu = B_\nu(T)$, the Planck function at the local temperature]. Equation (1) can then be recast in terms of the optical depth, defined so that $d\tau_\nu \equiv \rho\kappa_\nu ds$, and integrated to give

$$I_\nu = B_\nu(T)(1 - e^{-\tau_\nu}) \tag{2}$$

(see Rybicki & Lightman [1979] for a derivation). In this toy model, the continuum is simply blackbody radiation weighted by the absorbing column. Optically thick emission acts like a thermometer ($I_\nu \approx B_\nu$ when $\tau_\nu \gg 1$) for the $\tau \sim 1$ surface; optically thin emission probes the product of temperature,

[1] There are several Monte Carlo radiative transfer codes, designed for or amenable to studying disks, available as open-source software: RADMC-3D, HYPERION, MC3D, and MCMAX are commonly used examples (the latter two require contact with the developers for download). Other options (e.g., MCFOST) are available for collaborative work.

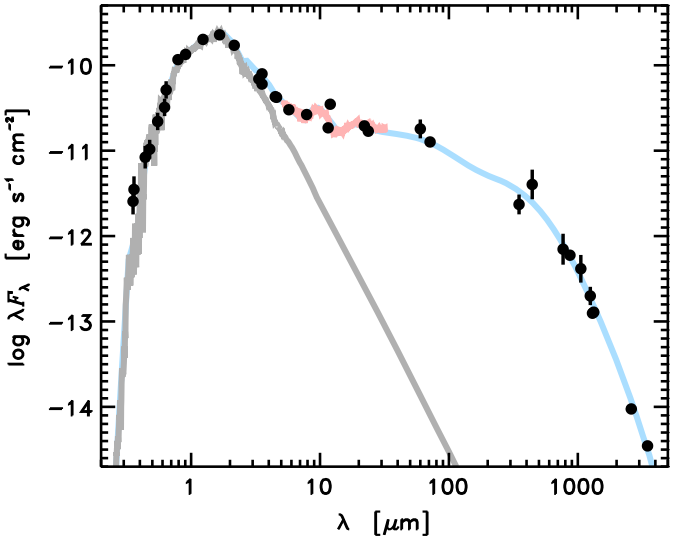

FIG. 2.—SED of the young star GO Tau and its associated disk (*black points*; data compiled by Andrews et al. 2013). Models of the stellar photosphere (*gray line*) and an illustrative dust disk (*blue line*; computed for a simple parametric structure using the RADMC-3D code) are also shown for reference, along with the *Spitzer* mid-infrared spectrum (*red line*; Furlan et al. 2009). See the electronic edition of the *PASP* for a color version of this figure.

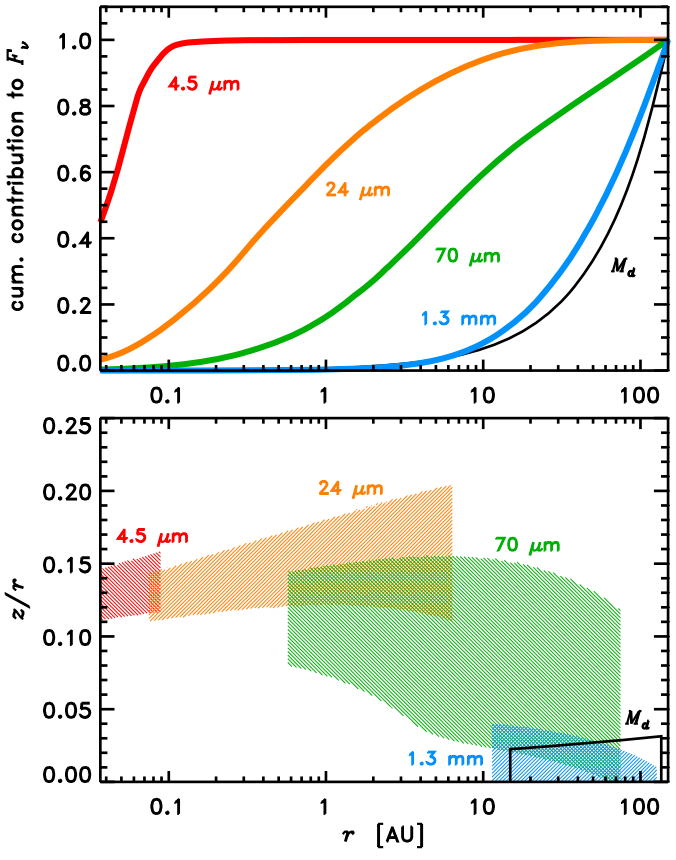

FIG. 3.—Top: Cumulative contributions to F_ν at four representative wavelengths as a function of r for the SED model in Fig. 2. The cumulative distribution of M_d is also shown (*black curve*). Note that the 4.5 and 24 μm curves are not zero at the inner edge, due to the stellar contribution. Bottom: Two-dimensional map of the regions that emit 80% of the flux (or enclose 0.8 M_d). See the electronic edition of the *PASP* for a color version of this figure.

column density ($N \equiv \int \rho ds$), and opacity ($I_\nu \approx \tau_\nu B_\nu$ when $\tau_\nu \ll 1$).

The SED is a basic tool for interpreting disk properties; an example is shown in Figure 2.[2] At ~1 μm, the SED is dominated by the host star. Thermal emission from the disk starts to outshine the star at $\gtrsim$2–5 μm, and peaks in the mid- or far-infrared. This emission is optically thick: its luminosity reflects the mean temperature and area of the emitting region, and its slope is related to the radial temperature gradient (Adams et al. 1987; Kenyon & Hartmann 1987; § 5.1). Broad spectral features (e.g., Fig. 2 near 10 μm) provide some insight on the dust mineralogy (e.g., Cohen & Witteborn 1985; Waelkens et al. 1996; Meeus et al. 2001; Kessler-Silacci et al. 2005; § 5.3). The turnover in the far-infrared marks the transition to optically thin emission. The luminosity at longer wavelengths scales with the product $\kappa_\nu B_\nu M_{\rm dust}$, where $M_{\rm dust}$ is the dust disk mass (Weintraub et al. 1989; Beckwith et al. 1990; Adams et al. 1990). The millimeter/radio SED slope probes the shape of the opacity spectrum (κ_ν; Beckwith & Sargent 1991; Mannings & Emerson 1994; § 5.3), itself a function of the compositions, morphologies, and sizes of the solids (e.g., Miyake & Nakagawa 1993; Henning & Stognienko 1996; D'Alessio et al. 2001; Draine 2006).

The nature of thermal emission ($\propto B_\nu$) means that shorter wavelengths preferentially trace warmer material. Since higher temperatures are usually found closer to the host star, the SED offers a qualitative $\lambda \mapsto r$ mapping (this is slightly complicated when the vertical dimension of the disk is considered; see § 5.1). Figure 3 provides a guide to the characteristic emission regions at four representative wavelengths, using the SED model in Figure 2. In the near-infrared, the emission is produced by both the innermost (~0.1 AU) part of the disk and the stellar photosphere (in this case, with nearly equal contributions). Since the inner disk densities are large and the near-infrared opacities are high, this emission is very optically thick; it originates in a layer that is a substantial height above the midplane. Mid-infrared emission has similar optical depths and probes material at large heights on radial scales of approximately a few AU. Far-infrared radiation is emitted over a larger range of radii and can become (partially) optically thin in the outer disk (approximately tens of

[2] The SED shows how energy, a useful physical quantity that characterizes the radiative transfer of starlight (and intrinsic energy) through the disk material, is distributed over frequency or wavelength. It is defined as νF_ν or λF_λ, rather than the practical, but physically meaningless, measurement of flux density, F_ν or F_λ ($= \int I_\nu d\Omega$). In a begrudging acceptance of standard jargon in the field, the latter is referred to as "flux" in this review.

AU). The low optical depths of the millimeter/radio emission offer unique access to cool material in the midplane.

In general, it is not possible to make unique, quantitative inferences about disk structures from SEDs alone. The reason is simple and fundamental. Disks are described by parameters that vary spatially (densities, temperatures) or mark specific geometries or locations (e.g., the viewing angle, inner/outer boundaries): constraints on such quantities from unresolved data are intrinsically ambiguous (see Thamm et al. [1994] or Chiang & Goldreich [1999] for practical demonstrations). That is not to claim that SEDs are useless diagnostics; indeed, sophisticated SED models have made crucial insights on disk properties (e.g., D'Alessio et al. 1998, 1999, 2001, 2006). But, the ability to alleviate or break some key structural degeneracies requires spatially resolved data.

That said, resolved observations of disks are not trivially obtained. Most nearby disks are located at distances of ~150 pc: there, the solar system dimensions subtend 0.″5 on the sky, and AU scales only ~0.″01. A quick examination of Figure 3 indicates that the thermal emission from a typical disk is confined well within the diffraction limits of ground and space-based telescopes. Interferometric measurements are the solution. Infrared interferometry offers unique insights on the inner disk structure at exquisite angular resolution (for more details, see the comprehensive reviews on the subject by Millan-Gabet et al. [2007] and Dullemond & Monnier [2010]); however, the emission at these wavelengths traces a minuscule fraction of the disk mass and extent (see Fig. 3). Instead, it is (sub)millimeter/radio interferometry that provides the most robust information on disk structure over the widest range of spatial scales. Contrary to a common misconception, observations at these long wavelengths are not solely probing the cool outer regions; with sufficient sensitivity and resolution (i.e., from ALMA), they will also provide rare access down to r of approximately a few AU.

Interferometers measure the Fourier transform of the brightness distribution at a discrete set of spatial scales, determined by the spacings between array elements and their projected motion onto the sky-plane as the Earth rotates. A complex "visibility" is measured at each scale; in a coordinate frame with the disk origin at the center, the real components are sensitive to the radial variation of the brightness, and the imaginary components record deviations from symmetry. The data are often displayed in condensed format, by azimuthally averaging into one-dimensional profiles that represent how the emission depends on spatial scale (Lay et al. 1994, 1997; Hughes et al. 2007): Figure 4 shows some examples. These profiles roughly correspond to the Fourier transform of the corresponding radial surface brightness profile. Recalling some Fourier transform pairs should clarify the behavior: a point source in the image domain has a constant amplitude in the visibility domain, a compact source has an extended visibility profile (and vice versa), and a ring-shaped source (§ 6.2) makes oscillations like a Bessel function. The visibilities are usually also inverted to construct an image (top panels, Fig. 4), but any analysis should usually be performed in the Fourier domain.

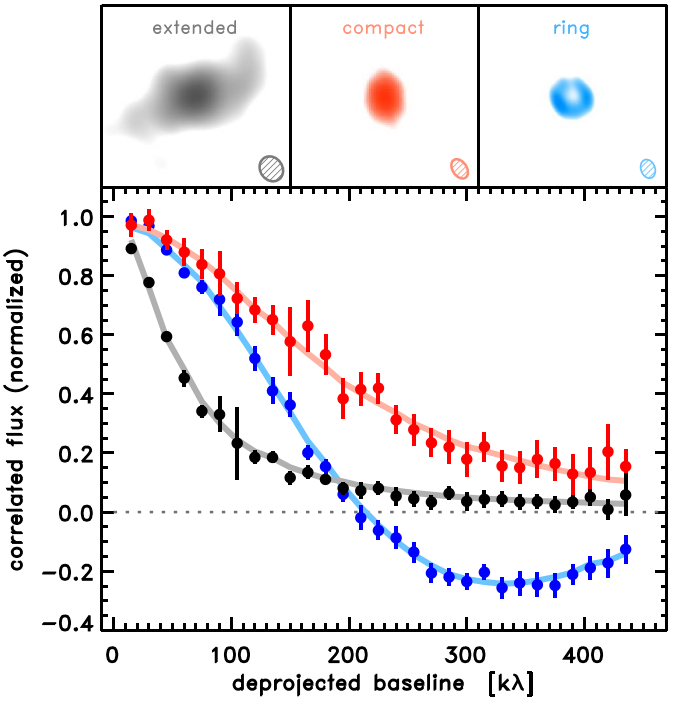

FIG. 4.—The 870 μm continuum visibility profiles (normalized real components, azimuthally averaged accounting for the viewing geometry projected onto the sky) for the GSS 39 (*black curve*), VSSG 1 (*red curve*), and SR 21 (*blue curve*) protoplanetary disks (Andrews et al. 2009). The corresponding images are shown in the top panels, with the synthesized beam dimensions marked in their lower right corners. See the electronic edition of the *PASP* for a color version of this figure.

3.2. Scattered Light

While the thermal radio emission is extraordinarily informative, it is not the only disk probe sensitive to a wide range of spatial scales. Scattered light, primarily in the optical and near-infrared, provides another key resolved diagnostic (see Watson et al. [2007] for a review); Figure 5 shows some examples of scattered light images. There is no pedagogical simplification for the radiative transfer equation when scattering is considered, since the source function is coupled to the radiation field.[3] Starlight is scattered by small dust grains with high albedos, having dimensions comparable to the spectral peak of the incident radiation field (~1 μm). The corresponding large scattering opacities mean that the observed emission originates in the disk surface layers and can be detected over a large range of disk densities (and therefore radial scales). Such observations are

[3] S_ν includes the integral of I_ν over angle, which requires an iterative numerical solution to eq. (1). This is not the case for pure thermal emission, where S_ν depends only on temperature (as was assumed in the approximation of eq. [2]).

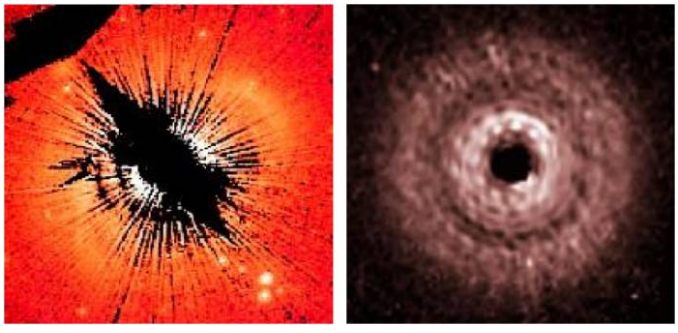

FIG. 5.—Coronagraphic images from *HST* showing the resolved optical and near-infrared starlight scattered off the surfaces of the disks around HD 163296 (left; Grady et al. 2000) and TW Hya (right; Debes et al. 2013), respectively. Some additional examples in different contexts can be found in Figs. 11 and 19. These images are reproduced with permission from the authors and the American Astronomical Society; © AAS. See the electronic edition of the *PASP* for a color version of this figure.

fundamental probes of vertical structure (§ 5.1) and can measure basic geometric parameters (e.g., inclination). Incorporating color and polarization data constrains the compositions, sizes, and shapes of the scatterers (§ 5.3).

The clear advantage of scattered light measurements is that they routinely achieve exquisite angular resolution (~0.″1 or less), making them well poised to identify and characterize ~10 AU scale substructure in disks (see § 6.2). The major challenge is contrast, since the host star is typically orders of magnitude brighter at the optimal scattering wavelengths. Coronagraphs or differential imaging techniques have been developed to mitigate such issues. Much of the current focus is on polarimetric differential imaging (e.g., Tamura 2009; Hinkley et al. 2009; Quanz et al. 2011; Perrin et al. 2015), which exploits the fact that direct starlight is unpolarized, but the scattering by dust grains can induce a significant polarization (Potter et al. 2000; Kuhn et al. 2001; Perrin et al. 2004). In practice, measurements of scattered light near the star are limited by subtraction residuals or coronagraph dimensions to ~0.1–0.″2 (the "inner working angle"). At larger radii, the data are typically sensitivity limited because of the diluted stellar radiation field (there is a $1/r^2$ depletion of scattering intensity on top of any intrinsic falloff caused by, e.g., a decreasing density of scatterers).

3.3. Synopsis

1. Solids (dust grains) dominate the disk opacity budget; observations of disks are most sensitive to the corresponding bright continuum emission.

2. Thermal emission is observed over a broad wavelength range; when optically thick, it measures the temperature in a surface layer, and when optically thin, it traces the product of temperature, density, and opacity (dust ensemble properties).

3. The morphology of the infrared SED is roughly related to the radial temperature distribution.

4. Spatially resolved data are mandatory to learn about disk structures; millimeter/radio interferometry measurements uniquely probe material in the midplane over a wide range of spatial scales.

5. Scattered light imaging is a complementary probe of resolved structure, especially sensitive to the vertical dimension and substructure on small scales.

Additional Reading: The first chapter of Rybicki & Lightman (1979); the review of some SED basics by Beckwith (1999); the summary reviews on disk measurements with millimeter/radio interferometers by Wilner & Lay (2000) and using scattered light images by McCaughrean et al. (2000) and Watson et al. (2007); the overview of disk observations by Hartmann (2008).

4. DEMOGRAPHICS

Planet formation research is still data-limited: the complexity of theoretical ideas outpaces observational constraints (although perhaps not for long). As in many similar areas of astrophysics, this means that progress is made in two complementary ways: (1) basic demographic studies for large surveys, and (2) in-depth analyses of individual (or small groups of) disks. This section focuses on the former. Case studies and detailed investigations of small samples are addressed in § 5 and 6.

Simple and practically accessible observational diagnostics are required to accumulate a sample large enough to quantify the statistical distribution of some property, or connections between properties, in a disk population. Key examples include the use of infrared photometry to describe the basic structural evolution of circumstellar material (Lada & Wilking 1984; Adams et al. 1987; Meeus et al. 2001; Robitaille et al. 2006; Evans et al. 2009) and the characteristic lifetime of warm dust in disks (Haisch et al. 2001; Hernández et al. 2008; see the summary by Mamajek [2009]). Simple accretion diagnostics, like the luminosity of the blue excess or the strength of a bright emission line, are also commonly employed to probe evolution (e.g., Hartmann et al. 1998; Sicilia-Aguilar et al. 2005) and disk–host relationships (e.g., Muzerolle et al. 2005; Natta et al. 2006).

From the perspective of planet formation, the disk mass (M_d) is a fundamental demographic parameter: in any theory, the efficiency of planet formation depends critically on the amount of raw building material available. Moreover, M_d can be estimated from a millimeter/radio flux measurement ($\propto M_{\rm dust}$; § 3.1), given some assumptions for (or ideally measurements of) the dust-to-gas ratio, dust opacity, and temperature.[4] This section

[4] For a dust-to-gas mass ratio ζ, the total disk mass is $M_d = M_{\rm dust}(1+\zeta^{-1})$, or $M_d \approx M_{\rm dust}/\zeta$ for a typical case where $\zeta \ll 1$.

addresses observational insights on the principal issues that affect disk masses, specifically the intrinsic relationship with host mass (M_*; § 4.1) and externally driven evolution through interactions with the local (§ 4.2) and global (§ 4.3) environment. A brief comment on what has been learned about the age-related evolution of the disk mass distribution is also made (§ 4.4).

4.1. Dependence on Host Mass

Most theoretical studies of planet formation assume that $M_d \propto M_*$. The intuition for this simple scaling relation follows from the star formation paradigm (cf., Shu et al. 1987), where a protostar accretes mass through its disk, which is fed by an envelope reservoir. The similar shapes of the observed core (envelope) and star mass functions affirm this kind of "gravitational" scaling (e.g., Motte et al. 1998; Enoch et al. 2006), but it need not apply to the intermediary disks. Even if a disk/host mass relationship was imprinted at the star formation epoch, it may not persist throughout its (potentially M_*-dependent) evolution up to the ages when disks become observable and form planets ($\gtrsim$1 Myr later).

And yet, the demographics of the exoplanet population offer compelling evidence in favor of such a relationship. Radial velocity surveys have demonstrated that the frequency of giant planets in compact ($\lesssim$few AU) orbits around nearby field stars scales linearly with host mass (Johnson et al. 2007, 2010; Bowler et al. 2010). Since the giant planet formation efficiency should roughly scale with the disk mass (e.g., Pollack et al. 1996; Hubickyj et al. 2005), this has been interpreted as strong, indirect evidence for a link between M_d and M_*.

The signature of that relationship was lacking in early millimeter/radio continuum surveys (e.g., Beckwith et al. 1990; Osterloh & Beckwith 1995; Andrews & Williams 2005), although the sampling in M_* was restricted to around 1 $M_\odot$. When extended to disks orbiting very low-mass hosts (~0.1 $M_\odot$), significantly fainter emission is measured (Klein et al. 2003; Scholz et al. 2006; Schaefer et al. 2009). A complete 1.3 mm continuum census across the host mass spectrum in the Taurus region confirms that the luminosities increase for hosts with earlier spectral types (Andrews et al. 2013), as demonstrated in Figure 6. For a fixed opacity, Andrews et al. (2013) found reasonable agreement with a linear $M_d \propto M_*$ scaling and a typical disk-to-host mass ratio of 0.2–0.6%. That said, there is substantial scatter around that relationship, with a 0.7 dex (factor of 5) dispersion in M_d at any given M_*.[5] Mohanty et al. (2013) independently verified this behavior with a different (incomplete, but partially overlapping) sample, and tentatively suggested that the relationship flattens (or perhaps even turns over) at high M_*. The same linear scaling is also consistent with the small survey of disk masses in the (older) Upper Sco association recently conducted by Carpenter et al. (2014).

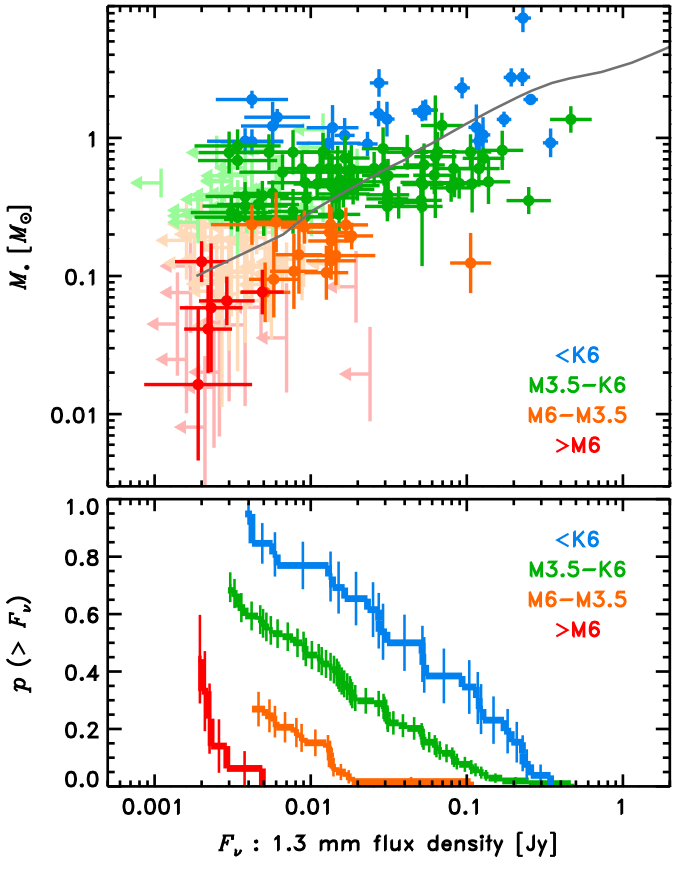

FIG. 6.—Top: The 1.3 mm continuum fluxes ($\propto M_d$) from Taurus disks as a function of their host masses (cf., Andrews et al. 2013). Upper limits on F_ν are shown as faded markings with left-pointing arrows. Despite considerable scatter, there is a clear correlation present that is consistent with a linear $M_d \propto M_*$ scaling; the gray curve shows such a relationship for the 2 Myr Siess et al. (2000) model isochrone and the Andrews et al. (2013) assumptions for linking F_ν and M_d. Bottom: Cumulative distributions for F_ν in four different host spectral type bins. These distributions are truncated by the survey sensitivity threshold at the low-flux end. See the electronic edition of the *PASP* for a color version of this figure.

It is tempting to link the observed scaling relations between M_d, M_*, and giant planet frequency. Assuming a direct mapping (for solar metallicity), and associating the giant planet frequency of ~$0.07(M_*/M_\odot)$ (Johnson et al. 2010) with the most massive disk progenitors, the Taurus disk mass distribution (Andrews et al. 2013) implies that giant planets form when $M_d \gtrsim 0.03\ M_*$. That mass threshold compares well with constraints in the solar system (Weidenschilling 1977b; Hayashi 1981; see § 5.2), and, coupled with the rough linearity of the scalings, is consistent with predictions of the core accretion theory for giant planet formation (Laughlin et al. 2004; Ida & Lin 2005; Kennedy & Kenyon 2008; Alibert et al. 2011; but see

[5] Note that this scatter means that some more complex relationships between M_d and M_* (rather than a simple power-law behavior) cannot be easily ruled out (Andrews et al. 2013).

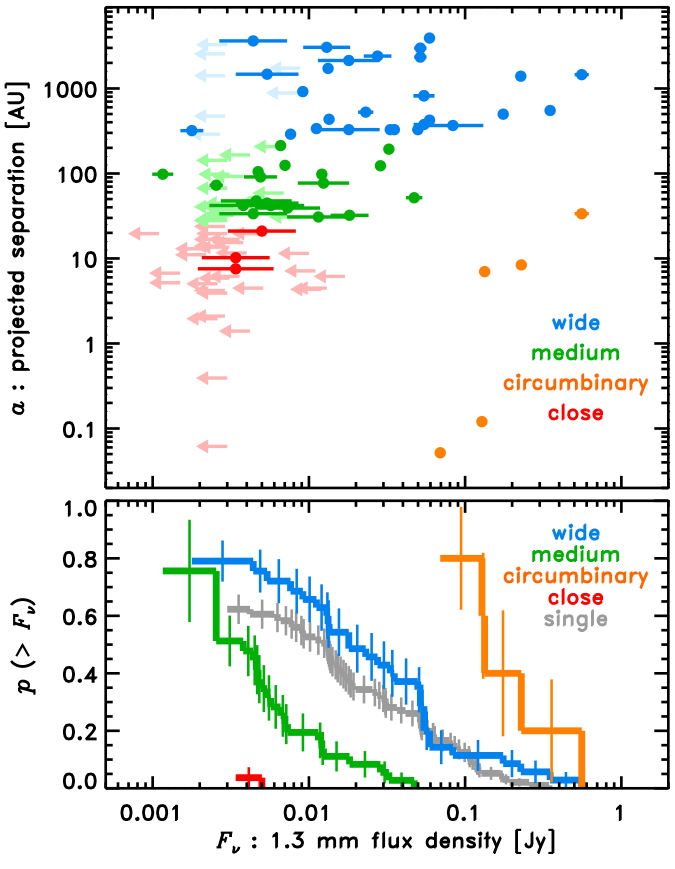

FIG. 7.—Top: The 1.3 mm flux ($\propto M_d$) from disks in stellar (spectral type ≤M5) multiple systems as a function of the separation between host pairs (cf., Harris et al. 2012; includes data from Akeson & Jensen [2014]). Symbols are as in Fig. 6. The flux distribution shifts to fainter values when the disks are hosted by closer pairs, although there is a bimodal distribution at the closest separations where circumbinary disks (*orange points*) can be especially bright (massive). Bottom: The cumulative distributions for F_ν in different pair separation bins. The *gray* distribution is for singles. See the electronic edition of the *PASP* for a color version of this figure.

Kornet et al. 2006). However, the inferred disk masses are considerably uncertain in an absolute sense (see § 5.2 and 5.3 for more details): aside from the notable scatter (Fig. 6), the opacities and dust-to-gas mass ratio are poorly constrained, and therefore, the conversion from observed emission (F_ν) to M_d may also be biased. If the inferred M_d values are systematically underestimated (by factors of a few), then the alternative disk instability mode of giant planet formation may also explain the linear scalings of disk/host/giant exoplanet properties (Boss 2011).

4.2. Effects of Host Multiplicity

Many stars are members of binary or higher order multiple systems (see the recent reviews by Duchêne & Kraus [2013] or Reipurth et al. [2014]). The multiplicity frequency for Sun-like stars is ~50% in the field (Abt & Levy 1976; Duquennoy & Mayor 1991; Raghavan et al. 2010), and may be even higher in nearby young associations (Leinert et al. 1993; Ghez et al. 1993; Reipurth & Zinnecker 1993; Simon et al. 1995; Kraus et al. 2011). Moreover, the distribution of orbital separations in multiples peaks near 100 AU (e.g., Raghavan et al. 2010; Kraus et al. 2011), comparable to the typical disk size (see § 5.2). Taken together, these properties suggest that the presence of a companion could play a decisive, general role in planet formation and the evolution of protoplanetary disks.

Dynamical interactions in multiple systems alter the structures of the associated circumstellar material: theoretical models indicate that tidal forces truncate individual disks at $r \gtrsim 0.2$–$0.5a$, where a is the orbital separation, and clear the inner regions of circumbinary disks at $r \lesssim 2$–$5a$ (e.g., Lin & Papaloizou 1993; Artymowicz & Lubow 1994, 1996). Despite such a disruptive environment, the mature counterparts of these young multiples are known to host planets (e.g., Patience et al. 2002; Raghavan et al. 2006; Desidera & Barbieri 2007; Bonavita & Desidera 2007). Observations of the disks in young stellar pairs offer key insights on how planet formation is affected in multiple host environments.

Given the predicted outcomes of these star–disk interactions, the observational focus has been on characterizing how disk properties vary with a (or its sky-projected equivalent). Seminal early work by Jensen et al. (1994, 1996) indicated that M_d is diminished for stellar pairs with $a \lesssim 50$–100 AU, in quantitative agreement with the expectations of tidal truncation models (see also Osterloh & Beckwith 1995; Andrews & Williams 2005; Cieza et al. 2009). Recent extensions of those studies with improved sensitivity confirm these results (Harris et al. 2012; Akeson & Jensen 2014): Figure 7 illustrates this behavior in the Taurus region. The closest pairs have lower disk masses (but see below) than those with wide separations or their singleton counterparts; the median M_d scales up by a factor of ~3 per decade in a. Similar conclusions are drawn from infrared excesses (e.g., Cieza et al. 2009; Kraus et al. 2012).[6] The frequency of short-period giant planets with binary hosts is also suppressed (Wang et al. 2014), consistent with this inferred disk mass depletion present at the planet formation epoch.

However, the separation-dependent pair demographics tell only part of the story. Component-resolved millimeter observations indicate that the primary disk almost always dominates the M_d budget, and that often the disk mass ratios are much different than would be expected from the standard theory, given the stellar masses and separations (Jensen & Akeson 2003; Patience et al. 2008; Harris et al. 2012; Akeson & Jensen 2014).

[6] However, as was highlighted in § 3.1, the high optical depths at such wavelengths make it difficult to link the results to mass depletion. Indeed, some studies find examples of infrared excess emission regardless of the projected host separation (e.g., White & Ghez 2001; McCabe et al. 2006; Pascucci et al. 2008).

Moreover, the resolved sizes of individual disks in such systems show, at best, marginal consistency with theoretical predictions for their tidal truncation radii (Harris et al. 2012). Aside from these apparent discrepancies, the pair demographics themselves highlight an additional (often unappreciated) mystery: unlike any other separation scale, there is a clear bimodal M_d distribution for the closest ($<$10 AU) pairs (see Fig. 7), with most remaining undetected, but a few having notably massive circumbinary disks.

Some of these observations might best be explained in terms of how the process of multiple star formation directs mass from the natal envelope to specific components in the system (i.e., initial conditions; Bate & Bonnell 1997; Bate 2000; Ochi et al. 2005). But there are also indications that the standard tidal interaction models are insufficient; modern hydrodynamic simulations suggest that asymmetries (like eccentricities or warps) are fundamental (e.g., Kley et al. 2008; Paardekooper et al. 2008; Marzari et al. 2009). Particularly striking are the systems with disks that are misaligned with respect to each other (Jensen et al. 2004; McCabe et al. 2011; Jensen & Akeson 2014; Williams et al. 2014) and/or the orbital planes of their respective hosts (e.g., Akeson et al. 2007; Verrier & Evans 2008; Andrews et al. 2010a).

4.3. Environmental Impact

Most disk observations are necessarily focused on the nearest star-forming regions, which have low stellar densities and few (if any) massive stars. However, most stars form in the significantly different environments of dense clusters (Lada & Lada 2003; Porras et al. 2003), where much larger stellar populations create opportunities for disks to be affected by two key external environmental factors. First, high stellar densities increase the probability for "fly-by" interactions, and thereby the tidal disruption of disks (e.g., Clarke & Pringle 1993; Korycansky & Papaloizou 1995; Larwood 1997; Boffin et al. 1998; Kobayashi & Ida 2001). Second, the high-mass tail of the M_* distribution is populated; disks in the immediate vicinity of massive stars will be depleted by photoevaporation, due to the locally intense radiation field (e.g., Hollenbach et al. 1994; Johnstone et al. 1998).

There is not yet any clear evidence indicating that tidal stripping from close stellar encounters plays a significant role in setting disk properties in rich clusters. Indeed, the expected interaction rate in the nearest massive cluster (the Orion Nebula cluster, or ONC) is quite small (e.g., Adams et al. 2006; Proszkow & Adams 2009). However, the relevant observational signature—a substantial radial truncation, and thereby mass depletion (e.g., Breslau et al. 2014)—is not yet readily available in the ONC or other, more distant, regions.

There is a wealth of data that probe the photoevaporation of disk material (around Sun-like hosts) in the proximity of massive stars, typically in the form of ionized (shocked) shell structures associated with silhouette disks (e.g., Churchwell et al. 1987; Bally et al. 1998a, 2000; Henney & O'Dell 1999; Smith et al. 2003). Early attempts to quantify the mass depletion in these disks with millimeter interferometry were difficult (e.g., Mundy et al. 1995; Bally et al.1998b; Eisner & Carpenter 2006), but eventually bore fruit at higher frequencies (Williams et al. 2005; Eisner et al. 2008). Mann & Williams (2009, 2010) identified a trend toward smaller disk masses for hosts located closer to the OB stars in the center of the ONC. Figure 8 shows a recent confirmation of this trend, which provides crucial quantitative evidence for photoevaporation-driven mass loss (Mann et al. 2014): stars located inside the region where energetic ultraviolet photons from the O6 star θ^1 Ori C dominate the radiation field ($\lesssim$0.03 pc) host only faint (low-mass) disks.

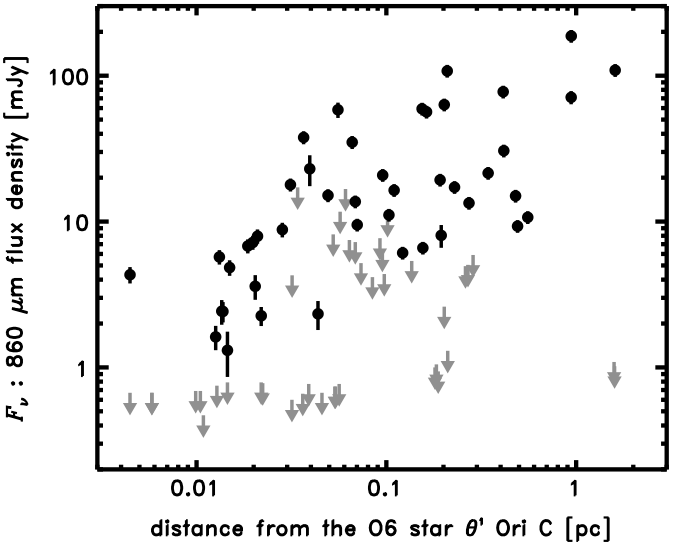

FIG. 8.—The 860 μm fluxes ($\propto M_d$) from disks in the ONC as a function of their projected separation from the massive star θ^1 Ori C (cf., Mann & Williams 2010; Mann et al. 2014). Upper limits (3σ) are marked with gray arrows. Disk masses drop precipitously when their hosts are located in the small region ($\lesssim$0.03 pc) where extreme UV emission from the Trapezium stars dominates the radiation field, as expected from photoevaporation models.

4.4. Mass Evolution

By the time they are observable, disks have already undergone some (perhaps substantial) evolution. The key signatures of that evolution will be covered in § 6, but the relevant timescales are best considered from a demographic perspective. The standard astronomical approach tracks how a given property changes between large samples that have different mean ages.[7] Application of this technique to simple disk tracers, like the infrared excess (e.g., Haisch et al. 2001; Hernández et al. 2007) or accretion rate indicators (e.g., Sicilia-Aguilar et al. 2010), suggests

[7] The ages of young stars are not well determined (see Soderblom et al. 2014). The benchmarks common in the literature and propagated here can be interpreted with considerable liberty.

that the typical inner disk (<1 AU) survives over a $\sim$5–10 Myr timescale (but see Pfalzner et al. 2014). But such constraints offer little in terms of assessing the available timeframe for planet formation. For that, it is critical to know the mass depletion rate, or how the M_d distribution changes with time.

The current observational information on M_d evolution is very limited. Only the Taurus region ($\sim$2–3 Myr) has a millimeter continuum census complete to a sufficiently deep limit (Beckwith et al. 1990; Osterloh & Beckwith 1995; Andrews & Williams 2005; Andrews et al. 2013). Continuum surveys are also available for the NGC 2024 (1 Myr; Eisner & Carpenter 2003; Mann et al. 2015), Ophiuchus (1–2 Myr; Andre & Montmerle 1994; Nuernberger et al. 1998; Andrews & Williams 2007a), ONC (1–3 Myr; e.g., Mann et al. 2014), Lupus (1–3 Myr; Nuernberger et al. 1997), Chamaeleon (1–3 Myr; Henning & Thamm 1994), MBM 12 (1–3 Myr; Hogerheijde et al. 2002), IC 348 (3 Myr; Carpenter 2002; Lee et al. 2011), σ Ori (3–5 Myr; Williams et al. 2013), λ Ori (5 Myr; Ansdell et al. 2015), and Upper Sco (5–10 Myr; Mathews et al. 2012; Carpenter et al. 2014) clusters, although with inhomogeneous sizes, completeness levels, and sensitivities. Comparisons between these samples are difficult, due to the strong selection effects related to the demographic trends discussed above; biased, small samples can mimic or obscure real evolutionary changes in the M_d distribution (Andrews et al. 2013). That said, the low detection rates in the oldest samples that have been probed (σ Ori, λ Ori, and Upper Sco, at $\sim$5 Myr) do indicate an overall decrease in the mean disk mass.

4.5. Synopsis

1. Disk mass is the fundamental aggregate property in planet formation models. The factors that influence M_d can be studied demographically with large millimeter/radio continuum photometry surveys, although they are subject to uncertainties in the assumed dust-to-gas ratio, opacities, and temperatures.

2. Disk masses are related to their stellar host masses; a roughly linear $M_d \propto M_*$ scaling seems appropriate, although there is a large dispersion (0.7 dex) in M_d for any given M_*. For standard assumptions, the median disk-to-star mass ratio is $\sim$0.2–0.6%.

3. In multiple star systems, close pairs tend to host low-mass disks. Most of the circumstellar material is usually concentrated around the primary star.

4. Disk masses are depleted (by photoevaporation) in the immediate vicinity of massive (OB) stars.

5. The timescales over which the M_d distribution changes are not yet clear, due to incomplete samples and selection effects. Preliminary results suggest that there is significant depletion within 5 Myr.

Additional Reading: The general review by Williams & Cieza (2011); the topical reviews of disk dissipation timescales by Hillenbrand (2008) and Mamajek (2009).

5. STRUCTURE

Although demographic studies reveal some fundamental properties of the disk population, their reliance on easy-to-observe "compound" diagnostics means that they cannot tell the whole story. An important complement is found in detailed probes of individual disk structures, which comprise a set of more "elemental" measurements. The single most valuable of these is the spatial distribution of mass. The efficiency of planet formation is directly linked to local disk densities: there must be enough stuff in the right places (for enough time) to assemble a planetary system from its progenitor (disk) material. Such a density threshold in solids is especially important in the formation models of terrestrial planets (e.g., Raymond et al. 2004; Kenyon & Bromley 2006; Kokubo et al. 2006) and giant planet cores (e.g., Mizuno 1980; Pollack et al. 1996; Hubickyj et al. 2005).

Inferring the disk structure from its associated observational tracers is complicated: there are elaborate dependences between the densities, temperatures, and material properties. Fortunately, different kinds of data are especially sensitive to specific aspects of disk structure (§ 3). When complementary tracers are considered together, they can be used to forge crucial benchmarks for models of planet formation and disk evolution. This section covers the key aspects of disk structures, with emphasis on the practical connections between physical parameters and data. It highlights the role of vertical structure in regulating the thermal budget (§ 5.1), the radial distribution of mass (§ 5.2), and the characteristic properties of the disk solids (§ 5.3).

5.1. Vertical Structure

5.1.1. Physical Overview

The aspect ratio of a rotationally flattened disk is small, $z/r \sim \mathcal{O}(0.1)$, since material is gravitationally concentrated at the midplane. But even this small vertical extent has important consequences. The most common model for a disk structure is based on some simple physical arguments for the gas, implicitly assuming that the solids follow the same distribution (but see § 6.1 for some important caveats). The underlying principle is that the disk is in vertical hydrostatic equilibrium,

$$\frac{\partial P}{\partial z} = -\rho g_z, \tag{3}$$

where P is the gas pressure, and g_z is the z-component of the gravitational acceleration. In most cases, the ideal gas equation of state is appropriate, and the stellar host dominates the potential. Equation (3) is then equivalent to

$$\frac{\partial \ln \rho}{\partial z} = -\left[\frac{\mu m_{\rm H}}{kT}\frac{GM_* z}{(r^2+z^2)^{3/2}} + \frac{\partial \ln T}{\partial z}\right], \tag{4}$$

with G is the gravitational constant, μ is the mean molecular weight, $m_{\rm H}$ is the mass of a hydrogen atom, and k is the

Boltzmann constant. Equation (4) is generally solved numerically, although some common simplifications enable an illustrative analytic solution. For a geometrically thin disk ($z \ll r$) with a small temperature gradient ($\partial T/\partial z \approx 0$), the solution to equation (4) is a simple Gaussian distribution,

$$\rho = \frac{\Sigma}{\sqrt{2\pi}H} \exp\left[-\frac{1}{2}\left(\frac{z}{H}\right)^2\right], \quad (5)$$

with

$$H = \frac{c_s}{\Omega} = \left(\frac{kT}{\mu m_{\rm H}} \frac{r^3}{GM_*}\right)^{1/2} \quad (6)$$

denoting a characteristic scale height (the ratio of the sound speed, c_s, to the Keplerian angular speed, Ω; cf., Shakura & Sunyaev 1973) and Σ representing a surface density (a boundary condition of the integration).

Simple energy arguments based on their observed bolometric luminosities indicate that disks are primarily heated by stellar irradiation (Adams & Shu 1986; Adams et al. 1987). With their large, broadband opacities maximized near the peak of the stellar spectrum, small (approximately micron-sized) grains are the most efficient conduit for that irradiation energy. Starlight absorbed in the disk surface layers heats those grains, which then re-emit some of that energy deeper into the disk interior to warm the midplane (Calvet et al. 1991, 1992; Malbet & Bertout 1991). This external deposition of energy produces a thermal inversion in the disk atmosphere (T increases with z) and modifies the vertical density distribution (cf., eq. [4]; Chiang & Goldreich 1997, 1999; D'Alessio et al. 1998, 1999; Bell et al. 1997; Bell 1999; Dullemond et al. 2001, 2002; Malbet et al. 2001). All else being equal, the heating depends on the irradiated area of the surface layer. If $H(r)/r$ is increasing, the tilt of this layer toward the star increases that area: such flared disks intercept more starlight than their flat counterparts, and therefore have warmer temperatures (at a given r; Kenyon & Hartmann 1987; Calvet et al. 1991; Chiang & Goldreich 1997). Figure 9 illustrates some examples of the relationship between the vertical distributions of ρ and T.

Although it is a simplification, equation (5) faithfully highlights this fundamental point about disk structures: the densities and temperatures are physically coupled. The intrinsic complexity of this coupling is that these physical conditions are linked to the radiative transfer of energy through the disk, which itself both depends on the densities and sets the temperatures. This feedback between structure and radiative transfer is a generic feature.

5.1.2. Observational Constraints

The most common approach used to measure the vertical structure of a disk employs the infrared SED as a diagnostic

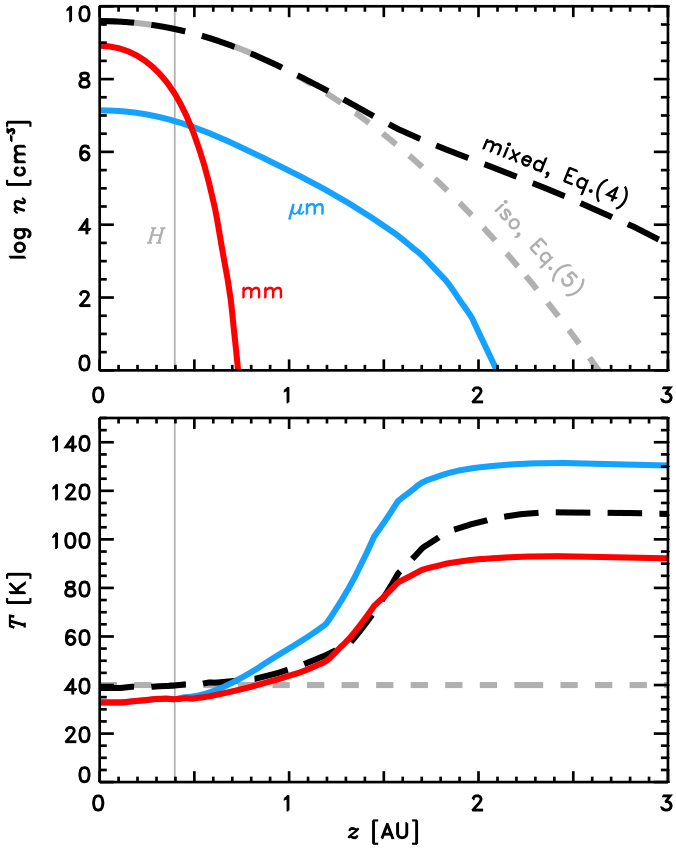

FIG. 9.—Vertical cuts at a fixed radius ($r = 10$ AU) of the density (top) and temperature (bottom) profiles for three illustrative disk structures. The simple vertically isothermal behavior described in eq. (5) is shown as gray dash-dot curves. The nominal scale height (corresponding to the midplane temperature), $H \approx 0.4$ AU, is marked with a vertical gray line. A more realistic variant, where particles with a power-law size distribution are well mixed with the gas and the vertical structure has been iterated using eq. (4) and a continuum radiative transfer code, is shown as *dashed black curves*. Finally, the *blue* and *red curves* represent particles with 1 μm and 1 mm sizes (respectively) from a similar model where the well-mixed assumption is relaxed: the solids are distributed according to a size-dependent balance between turbulent mixing and hydrostatic support, following the prescription of Dubrulle et al. (1995) (see § 6.1). All models use the same Σ and material properties and employ the RADMC-3D code. See the electronic edition of the *PASP* for a color version of this figure.

(cf., Fig. 3), and relies on modeling the connection between the height and temperature of the effective surface layer (the infrared "photosphere"; e.g., Kenyon & Hartmann 1987; Chiang & Goldreich 1997; D'Alessio et al. 1998). Since more energy is absorbed for a disk with a larger vertical extent, the temperature of the surface layer—and therefore the luminosity—scales with its characteristic height. The rough $\lambda \mapsto r$ mapping of the infrared SED (see § 3.1) means that the spectral slope reflects the radial variation of the surface layer height: more flaring makes a redder SED. Some examples of this effect are shown in Figure 10. However, although the SED does depend on the vertical structure, it alone cannot be used to unambiguously

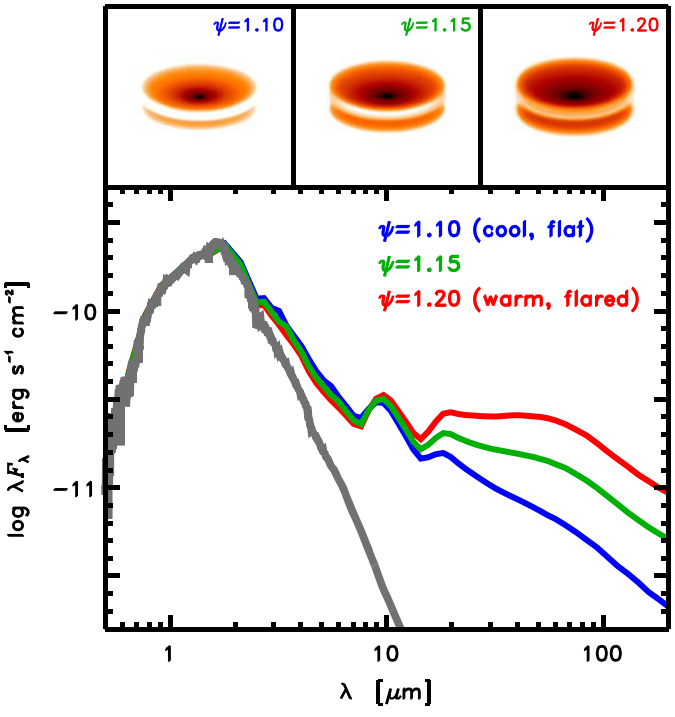

FIG. 10.—Demonstration of the impact that the characteristic height has on key observables, including scattered light (top) and the SED (bottom), using a simple structure model and the RADMC-3D code. The models have structures described by equation (5), with identical parameters aside from the shape of the radial H profile. Each $H(r)$ is normalized at 1 AU (to ~0.04 AU) and has a power-law scaling $H(r) \propto r^{\psi}$ with $\psi = 1.10$, 1.15, and 1.20. The most flared model ($\psi = 1.20$) exhibits brighter mid-infrared emission and has a more prominent scattered light disk. See the electronic edition of the *PASP* for a color version of this figure.

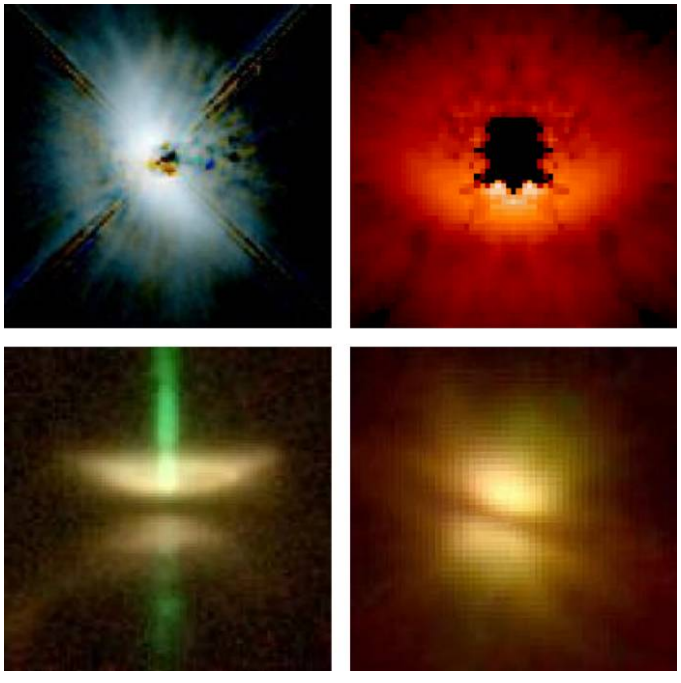

FIG. 11.—Examples of scattered light morphologies: (*clockwise, from top left*) optical/near-infrared *HST* images of GM Aur (Schneider et al. 2003), IM Lup (Pinte et al. 2008), HV Tau C (Stapelfeldt et al. 2003), and HH 30 IRS (Burrows et al. 1996; Watson & Stapelfeldt 2004, 2007; image courtesy of K. R. Stapelfeldt). These images are reproduced with permission from the authors and the AAS (© AAS) and *Astronomy & Astrophysics* (© ESO). See the electronic edition of the *PASP* for a color version of this figure.

quantify any associated physical parameters (e.g., H): again, unresolved tracers do not robustly measure spatial properties.

The most valuable complement is a resolved map of scattered light emission (§ 3.2). This emission generally appears as a bipolar pair of conical nebulae (representing the scattering layers on each side of the disk) with a dark waist (the disk interior); some representative examples are shown in Figure 11. The curvature, or opening angle, of these nebulae is set by the shape of the scattering surface and thereby the flaring geometry of the disk structure (e.g., Bastien & Menard 1990; Lazareff et al. 1990; Whitney & Hartmann 1992; Wood et al. 1998; D'Alessio et al. 1999; Takami et al. 2014). All else being equal, more flaring produces more curvature, larger nebulae, and a higher overall luminosity and polarization fraction for the scattered light. The images in Figure 11 illustrate some of these effects.

In practice, the inference of vertical structure parameters from such data relies on some assumptions (or external constraints) about the viewing geometry and optical properties of the scatterers. For intermediate inclination angles, these degeneracies are usually explored in a restricted forward-modeling process (Roddier et al. 1996; Close et al. 1998; Grady et al. 1999, 2000, 2007; Potter et al. 2000; Augereau et al. 2001; Krist et al. 2002, 2005; Schneider et al. 2003; Pinte et al. 2008; Kusakabe et al. 2012). Such ambiguities are diminished for extreme inclinations: the variation of the surface layer height with radius can be determined most directly from the nebular curvature in the edge-on case (e.g., Burrows et al. 1996; Lucas & Roche 1997; Krist et al. 1998; Padgett et al. 1999; Stapelfeldt et al. 1998, 2003; Cotera et al. 2001; Wolf et al. 2003; Perrin et al. 2006; Glauser et al. 2008), or more indirectly from the morphology of the radial brightness profile for face-on disks (e.g., Krist et al. 2000; Trilling et al. 2001; Debes et al. 2013).

Using equation (5) as a parametric structure, models of resolved scattered light data indicate $H/r \approx 0.05$–0.25, with only a modest radial variation ($\propto r^{0.1-0.3}$). Similar estimates are made from the infrared SED. As a point of reference, the hydrostatic solution for a vertically isothermal disk predicts that $H/r \propto r^{1/4}$. It is worth a reminder that these are not actually measurements of the pressure scale height H, but rather inferences based on constraints of the characteristic height of the surface layer where dust scatters or absorbs starlight (which are not necessarily colocated). Although these are expected to roughly track one another, there are some additional effects that impact their relationship (§ 6.1).

One such complication occurs when the characteristic height does not rise monotonically with r. If material closer to the star is distributed to sufficiently large heights, it can attenuate the radiation field at larger radii. This shadowing is usually attributed to a "puffed-up" inner disk edge (or wall), where internal energy generated by viscous dissipation (for disks with high accretion rates; e.g., D'Alessio et al. 1998) or direct irradiation of the inner disk edge (Natta et al. 2001; Dullemond et al. 2001; D'Alessio et al. 2005; Calvet et al. 2005) heats the material on sub-AU scales and inflates the local scale height. However, it may also be produced if vertical mixing is more vigorous in the inner disk (e.g., Dullemond & Dominik 2004a) or in the presence of small-scale substructures. Regardless of its origin, such obscuration makes the outer disk cooler, lowers the effective surface layer, and therefore reduces the infrared SED (particularly at longer λ; a vertically enhanced inner edge actually produces more near-infrared emission) and scattered light luminosity (Dullemond et al. 2001; Dullemond & Dominik 2004a). These effects have been inferred from SED morphologies (e.g., Meeus et al. 2001; Natta et al. 2001; Dominik et al. 2003; Acke et al. 2004). A more striking, direct confirmation is found in scattered light images that show the flared outer disk emerging out of a shadow at large r (e.g., Garufi et al. 2014).

Synoptic infrared photometry surveys are suggesting that small-scale vertical substructures may be common. Variability at some level is ubiquitous (see Cody et al. 2014), but the timescales observed in the mid-infrared are surprising: they are much shorter than expected for the disk regions being traced (approximately a few AU; see Fig. 3; Sitko et al. 2008; Morales-Calderón et al. 2009; Flaherty et al. 2012; Kóspál et al. 2012; Rebull et al. 2014). When near-infrared monitoring is also available, a "see-sawing" wavelength dependence has been observed, where the blue and red ends of the spectrum change in the opposite sense (Muzerolle et al. 2009; Espaillat et al. 2011). In rare cases, this variability can be mapped in multiepoch resolved scattered light observations (Stapelfeldt et al. 1999; Watson & Stapelfeldt 2007; Wisniewski et al. 2008). Models of the amplitudes, timescales, and wavelength dependence of the variability suggest an origin at sub-AU radii, where modulations of the vertical structure (due to quickly evolving nonaxisymmetric features, turbulence, or warps) shadow the disk at larger radii (e.g., Flaherty & Muzerolle 2010; Flaherty et al. 2013).

5.2. Radial Structure

5.2.1. Physical Overview

The radial variation of the density structure is encapsulated in the surface density profile $\Sigma(\equiv \int \rho dz)$. As was already noted, Σ is the most informative, essential aspect of disk structure. The shape of Σ controls not only the likelihood of planet formation, but also the initial orbits and subsequent migrations of any planets during their formation epoch (e.g., Kokubo & Ida 2002; Raymond et al. 2005; Miguel et al. 2011). Moreover, Σ offers an indirect snapshot of the mass and (angular) momentum flows that underpin the global structural evolution of disk material (e.g., Hartmann et al. 1998).

The standard theoretical models for $\Sigma(r)$ are again based on the gas physics (presuming that the solids will follow the gas distribution; but see § 6.1), using a balance of viscous and gravitational torques (Lin & Papaloizou 1980; Ruden & Lin 1986; Ruden & Pollack 1991; Stepinski 1998). For a thin Keplerian disk, Σ (and its evolution) can be determined by solving the viscous diffusion equation (Lynden-Bell & Pringle 1974)

$$\frac{\partial \Sigma}{\partial t} = \frac{3}{r}\frac{\partial}{\partial r}\left[\sqrt{r}\frac{\partial}{\partial r}(\sqrt{r}\nu\Sigma)\right], \tag{7}$$

where ν is the viscosity. There is a vast literature associated with accretion flows and angular momentum transport in disks that centers around solving equation (7) for a variety of viscosity distributions (see the reviews by Pringle 1981; Papaloizou & Lin 1995; Turner et al. 2014). The typical assumptions, at least in studies making connections to observational data (although see Hueso & Guillot 2005), are that mass loss occurs only through accretion onto the star and that the viscosity is a (time-independent) radial power-law, $\nu \propto r^{\gamma}$. The latter is motivated by the Shakura & Sunyaev (1973) prescription for turbulent viscosities in accretion disks, where $\nu \propto c_s^2/\Omega$. In this case, there are analytic similarity solutions to equation (7), with a Σ profile that behaves like a power law with an exponential taper at large radii,

$$\Sigma \propto \left(\frac{r}{r_c}\right)^{-\gamma} \exp\left[-\left(\frac{r}{r_c}\right)^{2-\gamma}\right]. \tag{8}$$

The characteristic scaling radius, r_c, and the normalization depend on time and the initial conditions (e.g., size, mass, and mass flow rate; Lynden-Bell & Pringle 1974; Lin & Pringle 1987; Hartmann et al. 1998).

Given the uncertainty in these accretion disk models, empirical approximations are often preferred. The most common is an old idea based on a simplistic reconstruction of Σ in the solar nebula, where the current planet masses are augmented back to solar composition and then smeared into annuli (e.g., Young 1901; Edgeworth 1949; Kuiper 1956; Cameron 1962; Alfvén & Arrhenius 1970; Kusaka et al. 1970). For such a minimum mass solar nebula (MMSN) disk, Σ is simply a truncated power law: the canonical Weidenschilling (1977a) construction of the MMSN is shown in Figure 12. Although there are fundamental conceptual flaws with the MMSN,[8] it remains a standard benchmark in the field.

[8] Primary among these is the assumption of a static nebula and planetary system, meaning the MMSN density profile is a time-integrated structure (a convolution of two unknown effects: the density evolution and the efficiency by which material is accreted into the planets) rather than an instantaneous snapshot like would be observed in real disks or properly applied to a planet formation model (see also Cameron 1988; Davis 2005; Desch 2007).

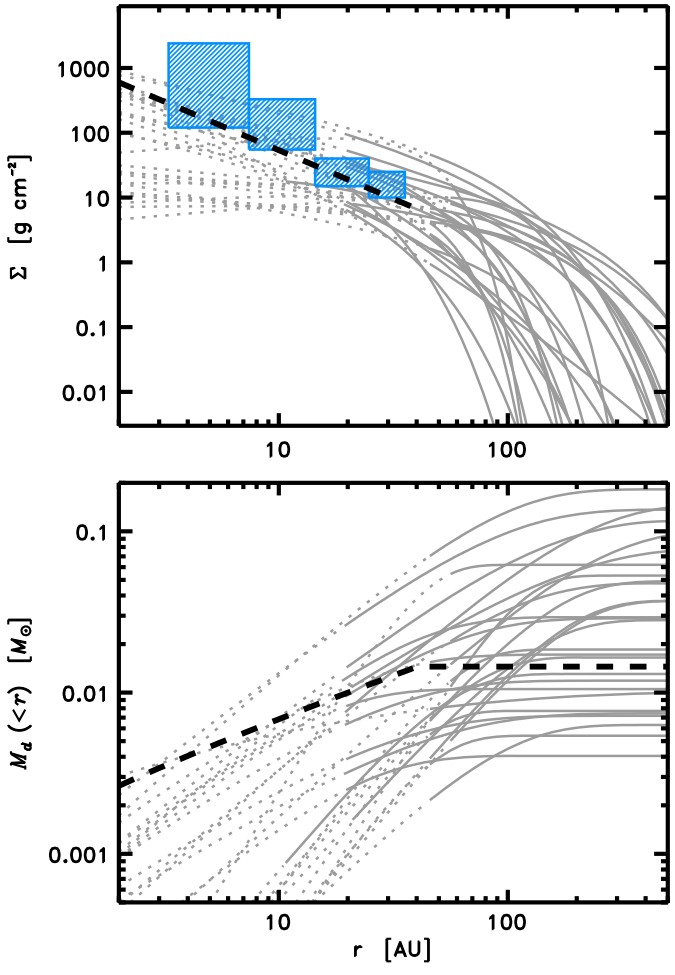

FIG. 12.—Top: The surface density profiles inferred from millimeter/radio interferometric observations of nearby disks (Andrews et al. 2009, 2010b, Isella et al. 2009, 2010a, Guilloteau et al. 2011), assuming a spatially homogeneous opacity spectrum, a 1% dust-to-gas ratio, and a similarity solution structure (cf., eq. [8]). These profiles are broken at spatial scales that are not directly resolved (i.e., where Σ has been extrapolated). Blue boxes mark the standard Weidenschilling (1977a) construction of the MMSN around the giant planets; the *dashed black curve* shows the normalization and shape advocated by Hayashi (1981). Bottom: Same information, but from the perspective of the cumulative mass distribution (the integrated mass inside some radius r). See the electronic edition of the *PASP* for a color version of this figure.

5.2.2. *Observational Constraints*

The most direct constraints on surface density profiles come from resolved (interferometric) observations of the (sub)millimeter continuum emitted by the disk solids (cf., § 3.1). Such emission typically has low optical depths, meaning the surface brightness scales with the product $\kappa_\nu B_\nu(T)\Sigma$. The standard approach to interpret the data is to assume that κ_ν is spatially homogeneous and then fit or solve for T (as a radial power law or with a radiative transfer calculation, respectively), and fit for Σ (as in eq. [8] or a power law), a characteristic or cut-off radius, and any other geometric parameters (e.g., inclination) with reference to the interferometric visibilities (e.g., Keene & Masson 1990; Lay et al. 1994, 1997; Wilner et al. 1996, 2000, 2003; Looney et al. 2000). For marginally resolved data, there are strong degeneracies between the radius parameter, inclination, and the radial gradients in T and Σ (e.g., Mundy et al. 1996). These can be mitigated with external constraints (the SED or scattered light data) on T and/or geometry (e.g., Akeson et al. 2002; Kitamura et al. 2002; Piétu et al. 2006; Hamidouche et al. 2006; Andrews & Williams 2007b; Pinte et al. 2008), but they persist at problematic levels unless the brightness distribution is resolved well.

For the nearest disk populations, a resolution of $\lesssim$0.″5 (60–70 AU) is usually sufficient to alleviate these degeneracies and place rudimentary constraints on Σ. Surface density profiles have been inferred with such data for a few dozen disks, primarily in the Taurus (Isella et al. 2009, 2010a; Piétu et al. 2006, 2014; Guilloteau et al. 2011) and Ophiuchus (Andrews et al. 2009, 2010b) regions (Fig. 12). With access to radii $\gtrsim$15–30 AU, these studies find a wide range of Σ gradients ($\gamma \approx 0$–1) and characteristic sizes ($r_c \approx 5$–200 AU);[9] some of that diversity reflects the different modeling approaches. Figure 12 also shows an alternative view in the form of cumulative mass distributions, which are perhaps more relevant for planet formation models. Many disks have roughly sufficient masses at 5–30 AU (based on model extrapolations) to form planetary systems like our own. However, the samples observed so far are biased (by necessity) toward the brightest, and thereby most massive, disks.

Andrews et al. (2010b) noticed an interesting trend, now confirmed by Piétu et al. (2014), that fainter disks are typically more compact; see Figure 13. This crude size-luminosity (mass) relationship could be a manifestation of initial conditions (diversity in core angular momenta) or viscous timescales (Andrews et al. 2010b); or perhaps it reflects variety in the evolutionary states of the solids (Piétu et al. 2014; see § 6.1 for further discussion). Following up on this trend is an active area of research, but larger samples and ancillary observations will be required to test hypotheses for its origins.

It is important to differentiate between what is being assumed and what is actually measured when interpreting resolved continuum data as described above. The surface brightness scales roughly with $B_\nu(1 - e^{-\tau_\nu})$ (eq. [2]), or $\sim B_\nu(T)\tau_\nu$ in the optically thin limit. A constraint on Σ requires a good (and internally self-consistent) model of the spatial variations of T (i.e., that the vertical structure and irradiation source properties are well determined) and opacity (recall $\tau_\nu = \kappa_\nu\Sigma$). For the latter, the typical assumption is that κ_ν is spatially invariant, which is

[9] There is an often unappreciated (although obvious) difference between cut-off radii in power-law models of Σ and the characteristic radii (r_c) in the similarity solutions (cf., eq. [8]): the latter encircle some significant fraction of the mass, but there is a non-negligible extension of low-density material at larger radii. Direct comparisons between different kinds of models require some care.

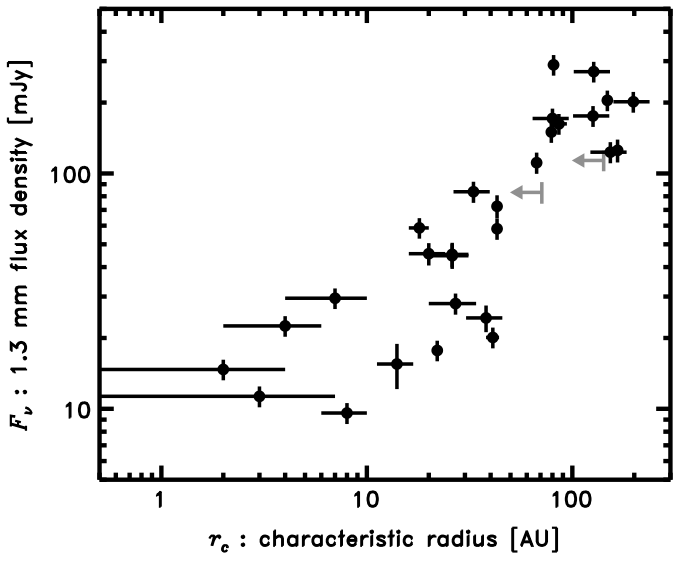

FIG. 13.—The 1.3 mm flux (scaled to a common distance), which scales with M_d, as a function of the characteristic radius r_c for all disks observed with a resolution better than $0\farcs75$ and modeled with the similarity solution prescription for Σ (eq. [8]). Measurements are from Andrews et al. (2009, 2010b), Isella et al. (2010a), Guilloteau et al. (2011), and Piétu et al. (2014) and exclude binaries (see § 4.2) and transition disks (see § 6.2).

not especially well justified (see § 5.3). In fact, radial and vertical variations in κ_ν are generally expected (§ 6.1), and therefore will impact any estimates of Σ and T. While there are other caveats in this line of work, it is these basic systematic uncertainties about the material properties of the solids that ultimately limit the ability to robustly constrain disk Σ profiles.

5.3. Material Properties

It should be obvious at this point that the links between observations and the physical properties of disks are fundamentally tied to the detailed interactions of their constituent solid particles with radiation. Those interactions are affected by the material properties of the solids, particularly their compositions, sizes, and morphologies. This information is parametrically encoded in the "optical" properties, absorption, and scattering opacities as well as scattering and polarization phase functions, that control the redistribution of radiative energy in both frequency and direction. These can be determined for any collection of particle properties and their corresponding optical constants (wavelength-dependent refractive indices) using numerical methods of varying sophistication, from simplified schemes like Mie theory (e.g., Bohren & Huffman 1983) to the brute-force simulated solutions of Maxwell's equations in the discrete dipole approximation (Purcell & Pennypacker 1973; Draine & Flatau 1994). The optical constants for many relevant materials have been calculated theoretically (e.g., Draine & Lee 1984; Laor & Draine 1993) or measured in the laboratory (e.g., Jaeger et al. 1994, 1998; Dorschner et al. 1995; Henning et al. 1995).

5.3.1. Particle Composition

Reasonable models for the composition of disk solids (e.g., Pollack et al. 1994) are based on assumed chemical pathways and abundance measurements in primordial solar system bodies (Lodders 2003): the primary contributors include silicates, carbonaceous materials, metallic compounds, and water ice. The emission bands at ~10 and 18 μm in disk spectra verify an abundant population of small silicate particles with a range of mineralogies (Forrest et al. 2004; Kessler-Silacci et al. 2005, 2006; Watson et al. 2009; Sargent et al. 2006, 2009a, 2009b; Olofsson et al. 2009; Oliveira et al. 2010, 2011). Additional features throughout the infrared provide evidence for hydrocarbons (polycyclic aromatic hydrocarbons; e.g., Habart et al. 2004; Geers et al. 2006, 2007; Keller et al. 2008), water ice (Chiang et al. 2001; Creech-Eakman et al. 2002; McClure et al. 2015), and other relevant minerals (e.g., Sturm et al. 2013). Resolved maps of scattered light colors suggest organic grain coatings (e.g., tholins; Debes et al. 2008, 2013; Rodigas et al. 2015). While it is not trivial to quantify the relative abundances of these materials, particularly in the midplane where spectral features are hidden by high optical depths, the combined constraints from disk spectra, analyses of meteorites, comets, and asteroids, and chemical intuition provide a reasonably coherent picture of the bulk composition of disk solids.

5.3.2. Particle Size Distribution

The particle size (radius), a, dictates the cross section for interaction with radiation of a given wavelength, and thereby has a significant impact on κ_ν. The opacity spectrum is approximately constant for $a \gg \lambda$ (geometric optics limit), falls off like λ^{-2} when $a \ll \lambda$ (Rayleigh limit), and is enhanced by resonant interactions at intermediate wavelengths. The implication is that emission observed at a given wavelength most efficiently probes particles of a similar size, $a \sim \lambda$. In a realistic disk environment, there will be a distribution of particle sizes, often approximated as a power law, $dN/da \propto a^{-q}$. Typically, most of the mass is in the largest particles ($q < 4$); as a reference point, simple collisional models (Dohnanyi 1969) and fits to the interstellar extinction curve (Mathis et al. 1977; Cardelli et al. 1989; Mathis 1990) suggest $q \approx 3.5$.

Figure 14 illustrates how the opacity spectrum changes for different particle size distributions. As the maximum size increases (or the distribution becomes more top-heavy), there are three general changes to the opacities. First, the infrared opacities decrease. However, if the disk is still optically thick in the infrared, it is not easy to demonstrate this observationally. Second, the silicate spectral features become muted (e.g., Min et al. 2004). This has been identified as a signature of grain growth in the disk surface layers (e.g., Bouwman et al. 2001; Meeus et al.

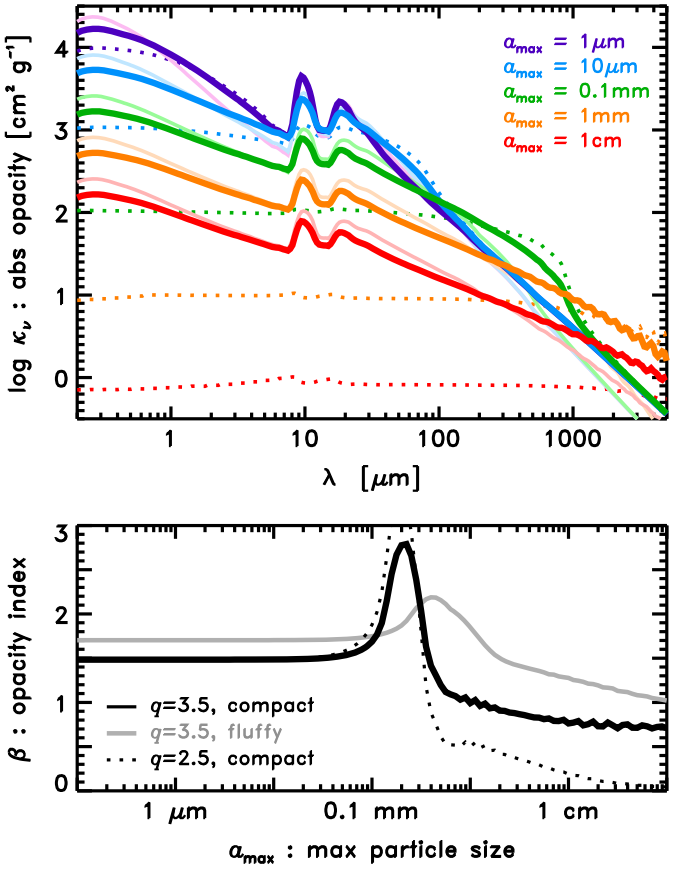

FIG. 14.—Top: Examples of absorption opacity spectra for simple models of dust populations relevant for disks, based on the homogenized analysis efforts of the DIsc ANAlysis (DIANA) project (P. Woitke, et al. 2015, in preparation). The composition is a mixture of amorphous silicates, carbon, and vacuum, with various assumptions about the size distribution and porosity (in this case, "compact" and "fluffy" mean filling factors of 1 and 0.5, respectively). Optical constants were collated from Dorschner et al. (1995) and Zubko et al. (1996) and combined using the Bruggeman (1935) mixing rule. The "distribution of hollow spheres" approach advocated by Min et al. (2005) was then used to compute opacities. Bottom: The 1–3 mm opacity spectral index, β, as a function of the maximum particle size. The typical spectral slopes measured for disks cluster around $\beta \lesssim 1$, indicating that most of the particle mass has grown to at least millimeter sizes. See the electronic edition of the *PASP* for a color version of this figure.

2001; Kessler-Silacci et al. 2006; Olofsson et al. 2009; Lommen et al. 2010), although there is room for structural (e.g., Dominik & Dullemond 2008) or compositional (Honda et al. 2003; Meeus et al. 2003) ambiguity in quantifying the size distribution. And third, the approximately power-law spectral behavior at millimeter/radio wavelengths flattens; i.e., if $\kappa_{\rm mm} \propto \nu^{\beta}$, then β decreases with larger $a_{\rm max}$ or smaller q (see Fig. 14; Miyake & Nakagawa 1993; Ossenkopf & Henning 1994; Henning & Stognienko 1996; D'Alessio et al. 2001; Draine 2006).

This latter point is especially interesting for disks because they become optically thin at these long wavelengths. The spectral dependence of the millimeter/radio continuum therefore scales with $B_\nu \kappa_\nu$; in the Rayleigh–Jeans limit the observed spectrum would scale like $\nu^{2+\beta}$, and so the radio "colors" serve as a key diagnostic of the particle size distribution.[10] For the small (submicron) grains in the interstellar medium, the millimeter/radio spectrum is steep; $\beta \approx 1.8 \pm 0.2$ (Hildebrand 1983; Goldsmith et al. 1997; Finkbeiner et al. 1999; Li & Draine 2001). The integrated spectra of approximately megayear-old disks have comparatively much "redder" colors, indicative of $\beta \lesssim 1$ in most cases (Beckwith & Sargent 1991; Mannings & Emerson 1994; Andrews & Williams 2005; Wilner et al. 2005; Lommen et al. 2007, 2009; Ricci et al. 2010a, 2010b; Ubach et al. 2012), and therefore, substantial growth ($a_{\rm max}$ is approximately millimeters or centimeters; e.g., Draine 2006). There are a few important points to keep in mind regarding the interpretation of spectral behavior in this context. For shallow spectra (low β), the relationship between the opacity spectral index and particle size saturates (see Fig. 14); when solids reach sizes much larger than the observing wavelengths, they emit much less and have negligible impact on the observed spectrum. So, associating β with a particle size distribution extending beyond centimeter-sized solids is generally not possible. More practically, it is crucial to spatially resolve brighter disks, so any contamination from optically thick emission (with a spectrum that scales like ν^2) can be identified (Testi et al. 2003; Natta et al. 2004; Rodmann et al. 2006; Ricci et al. 2012). Likewise, when increasing the spectral range to the radio ($\lambda \sim 1$ cm) in an effort to better leverage constraints on β, the contamination of nondisk emission (free-free or synchrotron radiation) also needs to be considered (e.g., Rodmann et al. 2006).

5.3.3. *Particle Morphology*

The optical properties of solids are also sensitive to their structure or morphology, typically discussed in terms of porosity (or the volume filling factor; e.g., Kozasa et al. 1992; Henning & Stognienko 1996; Min et al. 2003; Kimura et al. 2003; Ormel et al. 2011). Numerical simulations predict that small individual grains (monomers) will stick together in low-speed collisions and grow into fluffy, porous aggregates (e.g., Ossenkopf 1993; Dominik & Tielens 1997; Ormel et al. 2007; Wada et al. 2009; Okuzumi et al. 2012); laboratory experiments directly confirm this behavior (see Blum & Wurm 2008). The optical properties of porous aggregates depend on the product of their bulk size and filling factor (e.g., Kataoka et al. 2014). The absorption opacities of large aggregates with high porosity are similar to those for smaller, compact particles, with the subtle difference being that the resonant enhancement of κ_ν for $a \sim \lambda$ is muted (cf., Fig. 14). The corresponding scattering opacities may be relatively enhanced at long wavelengths: Kataoka et al.

[10] In practice, the Rayleigh–Jeans limit is often not strictly valid for disks. However, even simple assumptions for T can be used to appropriately account for the curvature in the Planck term.

(2014) suggest millimeter-wave polarimetry as a potential probe (although current limits are already quite strong; e.g., Hughes et al. 2009a, 2013). More information on the morphologies of disk solids is available, at least in the surface layers, through constraints on the scattering phase function (e.g., Mulders et al. 2013) and polarized intensities (e.g., Min et al. 2012).

5.3.4. Caveats on Mass and Density Estimates

On consideration of all these complex microphysical factors that set the opacities, which in turn are responsible for translating physical conditions into the astronomical tracers that are observed, the effort to quantify the role of disks in planet formation may seem incredibly daunting. And indeed, there is much work to be done in teasing out the complex interdependences between the material and structural properties of disks.[11] So, it is imperative to consider inferences about disk properties in the context of the assumed (i.e., model-dependent) properties of their constituent solids.

Given the fundamental significance of disk masses in the planet formation process, there is special interest in understanding the uncertainty (or diversity) in the opacities at millimeter wavelengths. With the few exceptions of disks with especially simple structures (e.g., Andrews et al. 2014), this issue is best assessed demographically. A few different arguments have been made that point toward the "standard" millimeter opacities ($\sim$2 cm^2 g^{-1} at 1.3 mm; Beckwith et al. 1990) being overestimated, and therefore that the disk masses may be higher than are typically inferred. One points out the order of magnitude mismatch between the masses inferred from the millimeter emission and a crude proxy using the product of accretion rates and ages (Hartmann et al. 1998, 2006). Another derives from the claim that the massive disk fraction seems to be too low to produce the observed giant planet frequency (e.g., Greaves & Rice 2010; Najita & Kenyon 2014).[12] The direction of this proposed uncertainty makes sense, since the growth of solids will lock up a fraction of the mass in large bodies that do not emit much at millimeter wavelengths (cf., Fig. 14). But its scale is perhaps less clear. It is unlikely that the masses could be substantially higher than estimated without a large population of gravitationally unstable disks, for which no evidence (e.g., Narayanan et al. 2006; Jang-Condell & Boss 2007; Dipierro et al. 2014) has yet been identified (see especially the symmetry for the very bright HL Tau disk; ALMA Partnership et al. 2015). So considering these (admittedly approximate) constraints, it seems reasonable to assume that the systematic uncertainty on the mean millimeter opacity in disks (relative to the typically adopted value) is modest, about $(\pm)1$ dex.

[11] The situation is in fact more complicated than presented, since the compositions, sizes, and morphologies of the solids all vary as a function of the physical conditions (e.g., see § 6.1).

[12] This discrepancy is not too large, since roughly a quarter of approximately megayear-old disks around Sun-like hosts have masses in excess of the MMSN (Andrews et al. 2013; Fig. 6). Nevertheless, it demonstrates that the masses are likely not systematically overestimated.

5.4. Synopsis

1. The flared, vertical distribution of dust grains regulates the thermal structure of a disk. The broadband infrared SED and spatially resolved measurements of optical/infrared scattered light can be used to constrain the vertical structure. In the context of simple models, such data suggest that the typical vertical aspect ratio ($\sim H/r$) is 0.1.

2. The radial surface density profile, Σ, is a crucial input for planet formation models. Interferometric measurements that resolve the optically thin millimeter continuum emission can be used to interpret the radial distribution of solid mass; some preliminary results are consistent with models of the (outer) primordial solar nebula.

3. The compositions, sizes, and shapes of the solid particles determine the opacities, which regulate the radiative transfer of energy into and out of the disk structure. There are strong and complex interdependencies between these material and structural properties. Measurements of the shape of the millimeter/radio continuum spectrum are sensitive to the particle size distribution; the relatively "red" millimeter/radio colors that are observed indicate the substantial growth of disk solids.

4. The physical conditions inferred from the interpretation of disk observations need to be considered only in the context of the model assumptions (e.g., the functional form of the density distribution, the material properties of the constituent solids).

Additional Reading: The review of disk modeling by Dullemond et al. (2007); a basic review of resolved structure constraints by Wilner & Lay (2000); the more general review by Williams & Cieza (2011).

6. EVOLUTION

The general framework for interpreting protoplanetary disk observations, as outlined in the previous sections, is still rather crude and oversimplified. With some recent enhancements in data quality, it has become clear that a more nuanced approach is necessary. There is now unequivocal evidence that evolutionary effects play a large (and likely dominant) role in determining the observable characteristics of these disks. The goal of this section is to highlight how two key evolutionary behaviors—the growth and migration of solids and the relatively rapid clearing of the inner disk—impact the standard observational benchmarks of disk structure, and thereby to point out opportunities for new insights on the physical mechanisms that drive such evolution.

6.1. Growth and Migration of Solids

Most observational studies of disk structures implicitly assume that the collisional evolution of the constituent solids

can be ignored. That is a bad assumption. The growth and migration of these solids involve extraordinarily complex processes, but exploring their consequences—both physically and observationally—is a crucial step toward developing a more comprehensive understanding of planet formation. To illustrate the effects of this evolution, in this section we will consider what happens to an "initial" population of small dust grains suspended in a (hydrostatically supported) gas reservoir with a homogeneous dust-to-gas ratio, $\zeta(r, z) = \zeta_0$.

6.1.1. Settling

Relative motions imparted stochastically (Brownian motion, turbulent mixing) will make these grains collide; at low speeds, they will stick together and produce larger aggregates (e.g., Blum & Wurm 2008; Güttler et al. 2010). Smaller particles are coupled to the gas, buoyed up into the disk atmosphere by hydrostatic support. But larger particles feel less of that lift and will settle toward the midplane (Adachi et al. 1976; Weidenschilling 1977a; Nakagawa et al. 1981). As they sink into denser regions, the collision rate increases and growth can accelerate. This growth and (vertical) migration feedback process is not perfectly efficient (Dullemond & Dominik 2005): alternative collision outcomes like electrostatic repulsion (Okuzumi 2009) and bouncing (Zsom et al. 2010) can slow growth, while fragmentation (Brauer et al. 2008; Birnstiel et al. 2009) and erosion (e.g., Seizinger et al. 2013; Krijt et al. 2015) can actually reverse it.

The interactions between the gas pressure, gravity, and (turbulent) mixing, coupled with the efficiency of particle growth (relative to destruction), gives rise to a size-sorted, sedimentary layering of the disk solids in which ζ decreases with z (e.g., Völk et al. 1980; Cuzzi et al. 1993; Dubrulle et al. 1995; Schräpler & Henning 2004). This size segregation increases the vertical temperature gradient and concentrates the absorption/scattering optical depth profile toward the midplane, reducing the irradiated surface area and height of the surface layer and thereby impacting some key observables (e.g., Dullemond & Dominik 2004b; see § 5.1).

A settled disk has a lower characteristic surface layer, absorbs less starlight, and therefore is colder. Consequently, it emits less thermal and scattered continuum radiation to the observer (Miyake & Nakagawa 1995; Dullemond & Dominik 2004b; D'Alessio et al. 2006; Mulders & Dominik 2012). Distinguishing settling from a disk with an intrinsically low gas pressure scale height, H, is not trivial. Some indirect constraints can be made from comparisons of mid-infrared colors and the strength of the $10\ \mu$m silicate feature (e.g., Kessler-Silacci et al. 2006; Furlan et al. 2009), or the inconsistent inferences of surface height layers from different tracers (e.g., scattered light images and infrared SEDs; Stapelfeldt et al. 2003; Wolf et al. 2003). A more direct signature of this stratification is accessible by comparing scattered light images at multiple wavelengths. Since dust grains preferentially scatter at wavelengths comparable to the particle size, settled disks show a scattering layer height that decreases with λ (Duchêne et al. 2003, 2004, 2010; Pinte et al. 2007; Gräfe et al. 2013). Edge-on disks may be particularly useful in future work on this subject, when ALMA can spatially resolve both the temperature structure of the gas (e.g., Dartois et al. 2003; Rosenfeld et al. 2013a; de Gregorio-Monsalvo et al. 2013) and the continuum that traces approximately millimeter particles as a function of height above the midplane (e.g., Boehler et al. 2013). As a reference, radiative transfer models of typical disk SEDs indicate that settling can reduce the dust-to-gas ratio in the disk atmosphere by a factor $1/\epsilon \approx 10$–1000, where $\zeta = \epsilon\zeta_0$ in the parlance of D'Alessio et al. (2006).

6.1.2. Radial Drift

Similar evolution also proceeds in the radial dimension. The radial motions of disk solids are fundamental to that evolution. Particles that are well coupled to the gas will follow its viscous flow trajectories, moving inward toward the host star at small radii (accretion), and away from it in the outer disk (diffusion) (e.g., see Takeuchi & Lin 2002). These radial velocities induced by viscous drag tend to be slow (approximately a few to tens of centimeters per second), and are most relevant for small (approximately micron-sized) particles. An aerodynamic process termed "radial drift" can be substantially more influential. In general, the gas motions in a disk are dominated by rotation around the host star. However, the presence of a radial pressure gradient imparts a small deviation from Keplerian velocities. For example, in the standard picture of a smooth disk with temperatures and densities that decrease with r, the pressure gradient is negative, and the gas disk rotates at a slightly sub-Keplerian rate. In the limit of weak coupling to the gas, solids orbit at Keplerian speeds. In the intermediate drag regime, particles with a certain range of sizes feel a strong headwind due to their velocity differential with the gas, which saps their orbital energy and sends them spiraling toward the pressure maximum (Whipple 1972; Adachi et al. 1976; Weidenschilling 1977a; Nakagawa et al. 1981, 1986). This radial drift moves solids so efficiently that they can be locally depleted faster than the coagulation timescale: in a MMSN disk, such a "drift barrier" to further growth occurs at $\sim$1 AU for meter-sized bodies, and at $\sim$100 AU for millimeter-sized particles.

The radial migration outlined above significantly modifies the distribution of disk solids in both size and space. Figure 15 illustrates these effects for a representative evolutionary model (cf., Birnstiel & Andrews 2014). The higher densities and relative velocities present at smaller disk radii naturally enhance the local collision (and thereby growth) rates (e.g., Dullemond & Dominik 2005). But the added influx of approximately millimeter/centimeter-sized particles from the outer disk will amplify this radial size-sorting. The net result is that larger solids will be preferentially concentrated close to the gas pressure maximum (typically the inner disk edge; e.g., Takeuchi & Lin 2002;

Brauer et al. 2008; Birnstiel et al. 2010, 2012). Since most of the solid mass is in larger particles that are systematically depleted from the outer disk by radial drift, the dust-to-gas ratio ζ decreases with r (Takeuchi et al. 2005; Birnstiel & Andrews 2014). For the sizes where drift velocities are maximal in the outer disk (approximately millimeter/centimeter), the ratio ($\zeta_{\rm mm}$) drops precipitously at ~10–100 AU (Youdin & Shu 2002; Weidenschilling 2003; Takeuchi & Lin 2005; Jacquet et al. 2012; Birnstiel & Andrews 2014).

6.1.3. Signatures of Radial Drift

These physical effects have pronounced observational hallmarks. The radial sorting of particle sizes induced by growth and drift is manifested in the disk opacities, κ_ν, particularly at millimeter/centimeter wavelengths (cf., § 5.3). Since larger particles have a lower opacity spectral index, β (a "redder" κ_ν), disks that have experienced substantial evolution in their solids will have an increasing $\beta(r)$: such an opacity profile is observed as a radial variation of the radio colors (i.e., a relatively "blue," or steep, spectrum at larger r; Isella et al. 2010a). In practice, this color gradient is observable as an anticorrelation between the wavelength and size of the continuum emission, such that the intensity distribution at longer wavelengths is more compact (Banzatti et al. 2011; Guilloteau et al. 2011; Pérez et al. 2012, 2015; Trotta et al. 2013; Menu et al. 2014). Figure 16 shows an example of this effect.

A confirmation of the related prediction that drift produces a decreasing $\zeta(r)$ (cf., Fig. 15) is more difficult, since accessing and interpreting gas density tracers remains a challenge. However, some indirect, qualitative evidence supporting a steep drop-off in $\zeta_{\rm mm}(r)$ is available through a comparison of the millimeter/centimeter-wavelength continuum and molecular line emission sizes: the former should have a more radially compact distribution than the latter. Such line/continuum size discrepancies have been noted for some time (e.g., Piétu et al. 2005; Isella et al. 2007), but were (reasonably) attributed to optical depth effects: since the millimeter/centimeter continuum is optically thin, insufficient sensitivity can lead to a size underestimate relative to the optically thick lines that typically trace the gas (Hughes et al. 2008). As the data quality has improved, it has nevertheless become clear that these apparent size discrepancies are not observational artifacts, but are instead intrinsic to the disk structures. For a still-limited sample, this signature of radial drift is manifested in a millimeter continuum distribution ~2–5× smaller than for the CO line (Panić et al. 2009; Andrews et al. 2012; Rosenfeld et al. 2013b; de Gregorio-Monsalvo et al. 2013; Walsh et al. 2014; see Fig. 16).

Some complementary information is encoded in the morphology of the millimeter continuum at larger radii. The steep drop in $\zeta_{\rm mm}(r)$ predicted theoretically to be a consequence of radial drift (e.g., Birnstiel & Andrews 2014; see Fig. 15) should produce a relatively sharp outer "edge" in the continuum distribution. That edge is clearly identifiable in the oscillatory structure

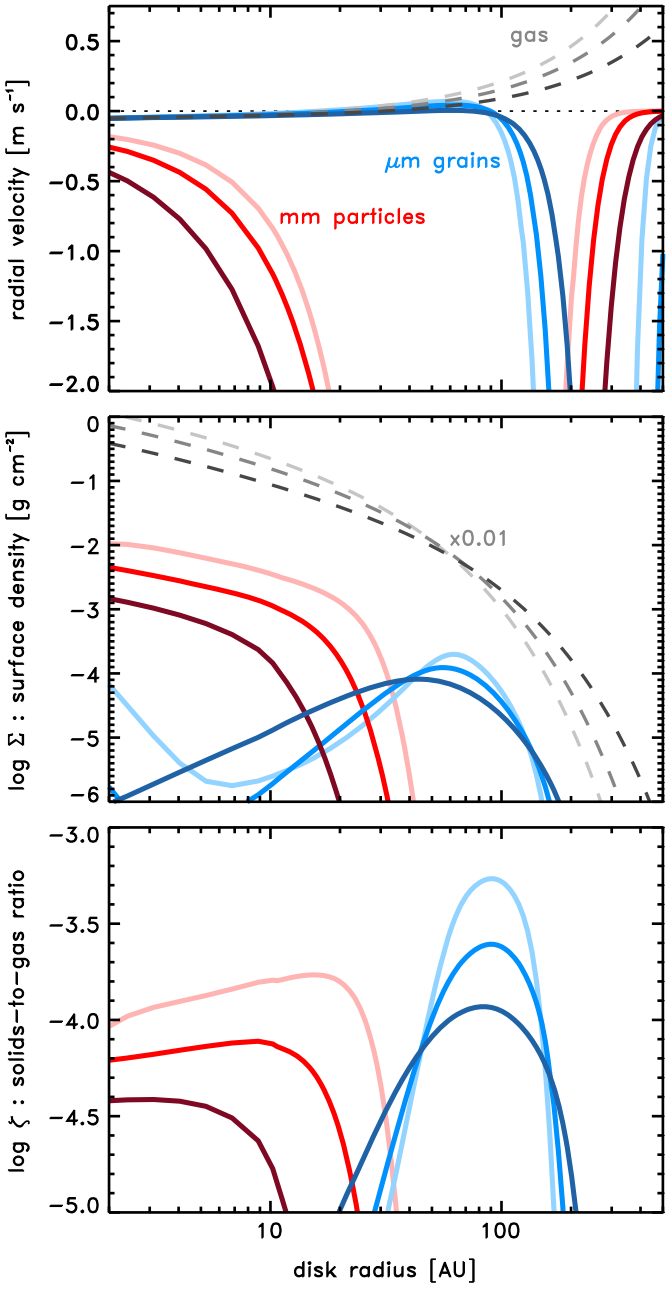

FIG. 15.—Demonstration of the evolution of solids embedded in a gas-rich disk. In each panel, grays refer to the gas, blues to approximately micron-sized grains, and reds to approximately millimeter-sized particles. Three time steps are shown—0.5, 1, and 2 Myr (from light to dark)—starting from an initial homogeneous distribution of submicron monomers with $\zeta = 0.01$ in a standard viscous accretion disk (see Birnstiel & Andrews [2014] for details). Top: Radial velocities: large negative (inward) motions (up to ~0.1 km s^{-1} levels) due to radial drift are noted for millimeter-sized solids at tens of AU. (Middle) Surface densities (Σ): the millimeter solids are radially concentrated and have a relatively sharp "edge" well interior to the gas or small grain distributions. Bottom: Dust-to-gas mass ratio (ζ): a steep drop in $\zeta_{\rm mm}$ is produced by radial drift. But note the scale in ζ: these low values are emblematic of a major issue with the radial drift timescales (they are much too short) in current evolutionary models. See the electronic edition of the *PASP* for a color version of this figure.

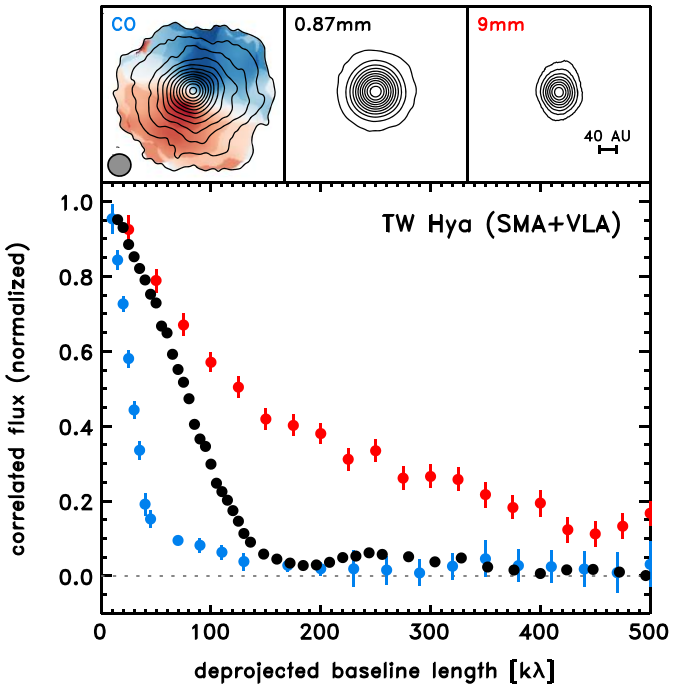

FIG. 16.—Illustration of the observational effects of particle growth and migration in the TW Hya disk. Top, left to right: The CO $J = 3 - 2$ line (color scale is the intensity-weighted velocity field), 870 μm continuum, and 9 mm continuum emission observed by the SubMillimeter Array (SMA) (Andrews et al. 2012) and Very Large Array (VLA) (Menu et al. 2014) interferometers. The images have the same scale (4″, ∼430 AU, on a side) and resolution (1″, ∼50 AU). Note the progression of radial concentration in the various tracers that is predicted by theoretical models (cf., Fig. 15). Bottom: The same progression from extended (CO) to compact (9 mm continuum), now viewed more directly as the azimuthally averaged visibility profiles (see § 3.1 and Fig. 4). The low-level oscillations in the 870 μm visibilities are a distinct signature of the "sharp" edge in the radial distribution of approximately millimeter-sized particles imposed by radial drift (see Fig. 15, bottom, and Birnstiel & Andrews 2014). See the electronic edition of the *PASP* for a color version of this figure.

it imprints on the interferometric visibilities (see Fig. 16; Andrews et al. 2012; de Gregorio-Monsalvo et al. 2013).

6.1.4. Open Issues

The dramatic modifications these evolutionary factors impart on the traditional observational tracers of structure (cf., § 5), should make it clear that constraining disk densities is a substantially more complicated task than has often been assumed. At some level, the spatial variations imposed on κ_ν and ζ by these evolutionary mechanisms render many of the standard assumptions used in the interpretation of disk structures invalid. To put it bluntly, there is not currently any obvious, coherent parametric framework available for characterizing the density distributions of disk solids. Right now, the focus is instead on collecting additional evidence that supports the evolution of solids, and building up a foundation for its proper interpretation. The expectation is that resolved multiwavelength continuum and spectral line data can be combined to better characterize the growth and migration of solids, and thereby to facilitate integrated studies of structure and evolution.

This subject is a relatively new, and incredibly dynamic, emphasis for the field. But while the influx of high-quality resolved data is qualitatively in sync with theoretical predictions for the growth and migration of disk solids, it is important to recognize that there are also some serious conflicts. Most prominent among these is the issue of migration timescales. Theory predicts that radial drift is much too efficient to explain the spatial distributions and luminosities of the millimeter-wavelength continuum that are routinely observed for approximately megayear-old disks (e.g., Takeuchi & Lin 2005; Brauer et al. 2007). The hypothesized remedy to relieve this tension is that there must be small-scale substructure in the gas disk (e.g., Whipple 1972; Pinilla et al. 2012b). Localized pressure maxima introduced by turbulent fluctuations (Klahr & Henning 1997; Dzyurkevich et al. 2013; Flock et al. 2015), magnetohydrodynamic (MHD) structures (i.e., zonal flows; Johansen et al. 2009; Bai & Stone 2014; Suzuki & Inutsuka 2014; Bai 2015), condensation fronts (e.g., Kretke & Lin 2007), or dynamical perturbations from (planetary) companions (Pinilla et al. 2012a; Birnstiel et al. 2013) can slow or even "trap" drifting particles, potentially reconciling the theoretical timescales and observational constraints. There is some preliminary evidence in support of these kinds of substructure for a special subset of disks (see § 6.2), and there will soon be data capable of quantifying its nature and prevalence in the more general disk population (see § 7).

6.2. The "Transition" Phase

6.2.1. Physical Overview

The evolution of angular momentum, through turbulent transport (Shakura & Sunyaev 1973; Lynden-Bell & Pringle 1974; Hartmann et al. 1998) or dissipation via magnetic winds (Blandford & Payne 1982; Konigl 1989; Bai & Stone 2013), largely dictates the long-term behavior of disk structures. If acting alone, such processes would steadily deplete the densities until the disk slowly (tens of megayears) faded away. However, there are additional mechanisms that should expedite the dissipation or transformation of the disk material.

In terms of dispersal, the primary pathway of interest is through a photoevaporative wind. Energetic radiation (far-ultraviolet to X-ray) generated by the host star can impart the gas in the disk surface with enough energy to escape the system (Clarke et al. 2001; Alexander et al. 2006a; Ercolano et al. 2008; Gorti & Hollenbach 2009; Owen et al. 2010). When the mass-loss rate in the resulting wind exceeds the (inward) viscous flow rate, a gap opens near the wind launch radius (approximately a few AU; e.g., Liffman 2003; Font et al. 2004; Ercolano et al. 2009). The inner disk is cut off from resupply, and will quickly ($\lesssim$0.1 Myr) accrete onto the star (∼0.1 Myr; e.g., Alexander

et al. 2006b; Gorti et al. 2009; Owen et al. 2011). This depletion makes the inner disk optically thin in the radial direction, permitting a more efficient irradiation at the inner edge of the remaining disk. This in turn enhances the wind mass-loss rate and thereby quickly ($\lesssim 0.01$ Myr) expands the wind-driven "cavity" at the disk center to $r \gtrsim 10$ AU (Clarke et al. 2001; Alexander et al. 2006b; Owen et al. 2012); it may even trigger an instability that destroys the disk altogether (Owen et al. 2013).

In the alternative (but not mutually exclusive; e.g., Matsuyama et al. 2003; Rosotti et al. 2013) context of metamorphosis, planet formation can also dramatically alter the disk structure on relatively short timescales. Once a planet is sufficiently massive (depending on the disk viscosity, but typically ~ 0.1–$1\ M_{\rm jup}$), it exerts torques that repel the local disk material away from its orbital radius (e.g., Goldreich & Tremaine 1980; Lin & Papaloizou 1979, 1993; Bryden et al. 1999; Kley & Nelson 2012). The net result is a narrow annulus of depleted densities, a gap. Depending on the local disk properties and planet mass, some disk material may continue to flow to the planet (or beyond it) in accretion streams (Artymowicz & Lubow 1996; Kley 1999; Lubow et al. 1999). A more massive planet accretes a larger fraction of this flow (e.g., Lubow & D'Angelo 2006), diminishing the resupply of the disk region interior to the gap, and thereby effectively creating a "cavity" at the disk center (e.g., Varnière et al. 2006; Crida & Morbidelli 2007; Dodson-Robinson & Salyk 2011; Zhu et al. 2011).

Theoretical models of these processes make some important and testable observational predictions. The most fundamental of these is that disk evolution should involve two timescales—a long stage where the processes related to momentum transport dominate, followed by a rapid "transition" phase where the disk structure is severely modified by interactions with winds and/or (giant) planets—that can be identifiable in simple demographic data (e.g., see Alexander & Armitage 2009). The disks in this latter evolutionary phase have a distinct structural feature: a central region of depleted densities. Such a structure necessarily imposes a pressure maximum just outside this low-density cavity, which may concentrate drifting solids in a ring-shaped "trap" (cf., § 6.1; e.g., Alexander & Armitage 2007; Pinilla et al. 2012a; Gorti et al. 2015). As with normal disks (cf., § 6.1), these solids leave behind a radially extended gas disk with a low dust-to-gas ratio. The shape of the pressure gradient around the maximum regulates the flow of material to smaller radii. If the gradient is not too steep, gas and smaller particles can pass through into the cavity; however, larger solids are filtered out of this flow and remain trapped near the pressure maximum (e.g., Rice et al. 2006; Paardekooper & Mellema 2006; Zhu et al. 2012, 2014). In a sense, the small amount of material in the cavity (or, rather, the flow rate of disk material through that pressure maximum), provides important clues to the physical mechanism(s) responsible for the depletion that is central to this transitional phase of evolution (e.g., Alexander et al. 2006b; Najita et al. 2007, 2015; Alexander & Armitage 2009; Owen & Clarke 2012).

6.2.2. Observational Signatures

The observational evidence for this rapid stage of disk evolution predates (and motivates) much of the theoretical work. In any young cluster, there is a small subpopulation ($\sim$1–10%) that lacks a near-infrared excess but still exhibits strong dust emission at longer wavelengths (Strom et al. 1989; Skrutskie et al. 1990). These transition disks are usually identified by the "dip" in their infrared spectra, with blue colors shortward of ~ 5–$10\ \mu$m and red colors at longer wavelengths (e.g., Brown et al. 2007; Cieza et al. 2007, 2012; Merín et al. 2010; Furlan et al. 2011). A representative example is shown in Figure 17. Given the rough $\lambda \mapsto r$ mapping between the spectrum and dust temperatures (§ 3.1), this "dip" signature suggests a substantial depletion of solids in the warm inner disk (Strom et al. 1989; Skrutskie et al. 1990; Marsh & Mahoney 1992, 1993; Calvet et al. 2002, 2005; Rice et al. 2003; D'Alessio et al. 2005). If all disks experience such a transition, a simple duty cycle argument demands that it occurs quickly (the product of the transition disk fraction and the mean sample age, so $\lesssim 0.1$–0.5 Myr; but see Sicilia-Aguilar et al. 2008; Muzerolle et al. 2010). Comparing that rough timescale with the decay time of infrared excesses in the general disk population (§ 4.4; see Mamajek 2009), these simple infrared color demographics clearly reveal the theoretically predicted two-timescale behavior for disk evolution.

Moreover, the "dust ring" structures implied by these distinctive spectral morphologies have been directly confirmed, and characterized in detail, using resolved observations of the millimeter continuum (e.g., Piétu et al. 2005, 2006; Hughes et al. 2007, 2009b; Brown et al. 2008, 2009, 2012; Isella et al. 2010a, 2010b; Andrews et al. 2009, 2010b, 2011; Cieza et al. 2012; Mathews et al. 2012; Casassus et al. 2013; Fukagawa et al. 2013; Rosenfeld et al. 2013b; Tsukagoshi et al. 2014; Osorio et al. 2014; Huélamo et al. 2015; Canovas et al. 2015). Some illustrative examples are shown in Figure 18 (as well as the insets in Fig. 17). Resolved studies of transition disks have so far used haphazard selection, and are severely limited by luminosity and resolution constraints. The current sample shows cavities with radii of ~ 15–100 AU and emission levels suppressed by at least a factor of ~ 100, surrounded by bright, narrow rings (not well resolved; potentially with high optical depths). These morphological features are surprisingly more common than the infrared-based transition disk phenomenon in general, representing a quarter or more of the disks in the bright half of the millimeter luminosity (disk mass) function (Andrews et al. 2011). It is not yet clear how much this apparent discrepancy is influenced by the strong selection biases (i.e., bright sources only) in the resolved millimeter continuum sample.

The simple "dust ring + cavity" model for a transition disk structure becomes more complicated when additional tracers are considered. The presence of a small infrared excess (and often

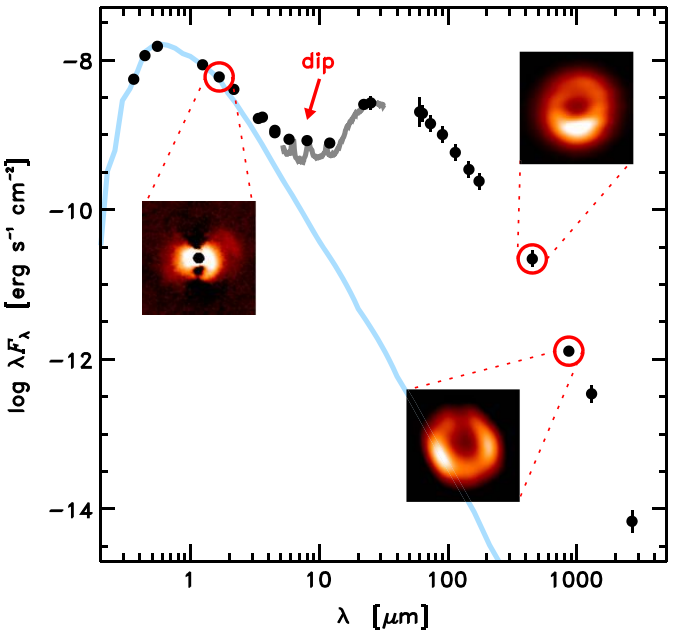

FIG. 17.—SED and representative resolved images of the transition disk around the young star SR21. The *blue curve* is a model of the stellar photosphere; the *gray curve* is a well-sampled spectrum from *Spitzer*. The SED shows a prominent "dip" in the infrared, produced by the substantial depletion of a cavity with radius ~20 AU. The image insets show the 1.6 μm (polarized) scattered light (Follette et al. 2013), along with the 450 μm (Pérez et al. 2014) and 870 μm thermal continuum emission (Brown et al. 2009). Each image spans 175 AU on a side. The thermal images clearly show the low-density cavity, but there is scattered light tracing small grains located well inside the (sub)millimeter ring. See the electronic edition of the *PASP* for a color version of this figure.

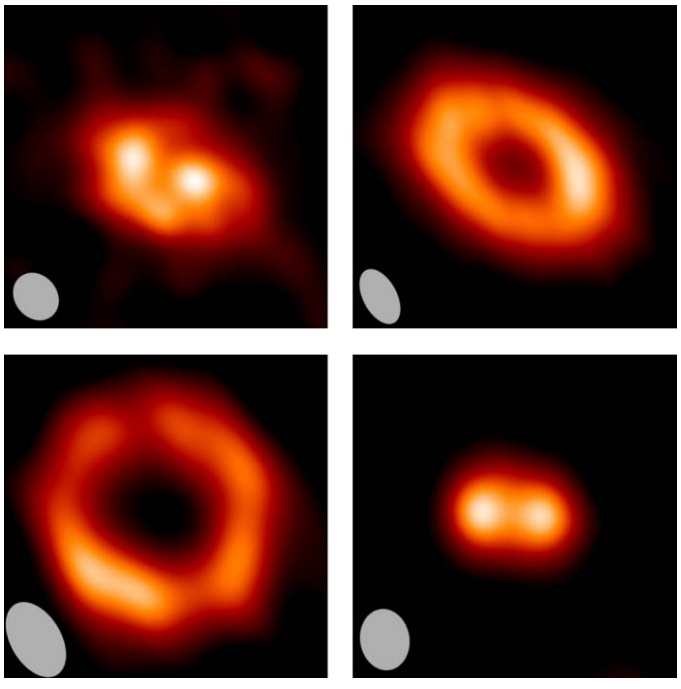

FIG. 18.—Examples of the 870 μm thermal continuum ring morphologies observed for transition disks (at various inclinations): (Clockwise, from top left) GM Aur (Hughes et al. 2009b), LkCa 15 (Andrews et al. 2011), RX J1633.9−2442 (Cieza et al. 2012), and RX J1604.3−2130 (Mathews et al. 2012). The synthesized beams are shown in the lower left of each panel. See the electronic edition of the *PASP* for a color version of this figure.

silicate emission features) in transition disk SEDs demonstrate that the cavities are not empty; rather, a "gapped" structure, with an additional band of small dust grains located near the host star, may be a more appropriate description (e.g., Espaillat et al. 2007, 2008, 2010). Since even a low mass of small particles can emit strongly in the infrared, such structures can even wash out the characteristic SED "dip" signature (e.g., Isella et al. 2010a, 2010b; Andrews et al. 2011). Moreover, spatially resolved observations of infrared scattered light (Dong et al. 2012; Hashimoto et al. 2012; Follette et al. 2013; Rapson et al. 2015; see Fig. 17 inset) and submillimeter emission (e.g., Pinilla et al. 2015) find smaller particles interior to the millimeter continuum rings, in some cases nearly filling the cavities.

These trace populations of small particles are clearly accompanied by gas. The accretion rates onto the transition disk hosts tend to be comparable to or slightly below those for more typical disks (Najita et al. 2007, 2015; Fang et al. 2009; Espaillat et al. 2012; Ingleby et al. 2014; Manara et al. 2014), suggesting that the mass flow is relatively uninterrupted by the gap(s) or cavity. Supplementary signatures of this gas reservoir are found in infrared rovibrational lines of common molecules located at few AU-scales (e.g., Salyk et al. 2009), unresolved emission in the wings of millimeter rotational lines (Rosenfeld et al. 2012), as well as direct spectral imaging of those same lines (Casassus et al. 2013; Fukagawa et al. 2013; Bruderer et al. 2014; Zhang et al. 2014; Pérez et al. 2015; Canovas et al. 2015; van der Marel et al. 2015). As with the small grains, constraints on the gas densities in the cavity are rudimentary. The bulk of the gas mass remains confined to the extended structures that reach well beyond the millimeter continuum rings (Hughes et al. 2009b; Resenfeld et al. 2013b; Walsh et al. 2014).

Considering all these observations together, there is strong empirical evidence supporting the theoretical model that transition disk structures are largely controlled by a narrow, radial (ring-like) gas pressure maximum located outside a zone of substantially depleted densities. For the specific examples that have been studied in detail so far, the measured accretion rates and cavity contents indicate that the pressure gradient outside the cavity is not too steep. Such properties are generally inconsistent with the predictions of photoevaporation models (Alexander & Armitage 2009; Owen & Clarke 2012), and so the operating hypothesis is that the observed structures are produced by dynamical interactions with very faint (e.g., Pott et al. 2010; Kraus et al. 2011), presumably planetary-mass, companions (although more massive stellar companions must be ruled out; e.g., Ireland & Kraus 2008). That is certainly an exciting prospect, and is naturally driving rapid developments in the pursuit for details

on these specific disks. A few putative planetary-mass candidates have even been identified inside transition disk cavities (e.g., Huélamo et al. 2011; Kraus & Ireland 2012; Reggiani et al. 2014; Biller et al. 2014; Quanz et al. 2015). That said, it is important to recognize that the subpopulation of disks receiving most of the attention is still biased (in terms of millimeter luminosity, cavity size, etc.): a larger swath of the disk population may have its properties shaped more by other evolutionary factors (e.g., photoevaporation).

6.2.3. Substructure

A particularly active topic of research on these disks is the characterization of their substructure, deviations from the simple one-dimensional (radial) description outlined above. From a phenomenological perspective, three basic types of substructure are observed in transition disks: azimuthal asymmetries, spirals, and warps. A prominent example (for two of these) is shown in Figure 19. The former type is common in the limited samples available, with the millimeter emission rings in some cases appearing lopsided: azimuthal contrast levels range from modest (a factor of $\lesssim$2; Brown et al. 2009; Isella et al. 2013; Rosenfeld et al. 2013b; Pérez et al. 2014) to extreme (a factor $>$30; Casassus et al. 2013; van der Marel et al. 2013; Fukagawa et al. 2013), and the asymmetries themselves can account for $\sim$30–100% of the integrated flux. These asymmetric features are azimuthally resolved (spanning tens of degrees), but radially narrow ($\lesssim$10–20 AU). The currently favored explanation for such substructure is the concentration of solids in an azimuthal gas pressure enhancement (Birnstiel et al. 2013), presumably driven by vortex instabilities produced exterior to the orbit of a perturbing companion (e.g., Barge & Sommeria 1995; Klahr & Henning 1997; Wolf & Klahr 2002; Regály et al. 2012; Lyra & Lin 2013; Zhu et al. 2014; Zhu & Stone 2014).

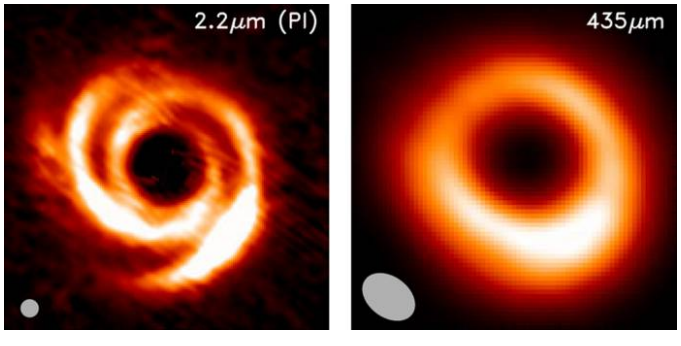

FIG. 19.—An especially dramatic example of substructure in the SAO 206462 transition disk. Left: The 2.2 μm (polarized) scattered light shows prominent spiral structure (Garufi et al. 2013). Right: The thermal continuum emission at 435 μm reveals a strong azimuthal asymmetry in the ring, which may be related to an unresolved spiral pattern (Pérez et al. 2014). Both images are on the same scale (200 AU on a side), with resolutions on the lower left. See the electronic edition of the *PASP* for a color version of this figure.

However, vortices are not the only viable explanations for the observed asymmetries; in some cases, they may alternatively be generated by global gravitational modes (Mittal & Chiang 2015), eccentricity (Kley & Dirksen 2006), or unresolved spiral structures (e.g., Pérez et al. 2014). The latter is of special interest, since remarkable spiral patterns have been observed in (usually polarized) scattered light from many of the transition disks with early-type hosts (a sensitivity-related selection bias). Both well-ordered, open spirals (e.g., Muto et al. 2012; Grady et al. 2013; Garufi et al. 2013) and more complex, tightly wound patterns (e.g., Clampin et al. 2003; Fukagawa et al. 2004, 2006; Canovas et al. 2013; Avenhaus et al. 2014) have been identified, typically extending from the inner working angles ($\sim$10 AU) out to $\gtrsim$100 AU scales. Some debate remains about the origins of these patterns, as true density waves (Dipierro et al. 2014, 2015) or manifestations of vertical substructure (Juhasz et al. 2015), but the forthcoming resolution improvements at millimeter wavelengths should settle the issue. Some care has to be taken in interpreting scattered light images, since the illumination pattern of the outer disk surface can also be affected by warped geometries (e.g., Roberge et al. 2005; Quillen 2006; Hashimoto et al. 2011; Marino et al. 2015). Resolved spectral line data bolsters the evidence that such vertical substructure may be a common feature in transition disks (e.g., Rosenfeld et al. 2012, 2014; Perez et al. 2015).

With new access to ALMA and high-quality (polarized) scattered light data, the past few years have seen rapid development in resolved studies of transition disks. The new signatures of dynamical substructure in these disks are marshaling a major investment in both observations and theoretical work. Ultimately, the goal is to provide firm, predictive links between the observed disk structures and the properties of the planetary perturbers that shape them, with results that have fundamental impacts on models of early planetary system architectures, migration, and the planetary accretion process. At the same time, it is beneficial to understand that the "sample" being studied so extensively is certainly biased: after all, these accreting, millimeter-bright disks with large and partially filled cavities are but a small subgroup of the general transition disk population (e.g., Cieza et al. 2008). It will be interesting to see how the description of transition disk structures changes when a more diverse sample is analyzed using data of similar quality.

6.3. Synopsis

1. Disk solids grow and migrate toward the local maximum in the gas pressure distribution. The result is a vertically and radially size-sorted density structure, with higher concentrations of larger particles at the midplane and in the inner disk. The vertical stratification can be observed in the infrared SED, or through multiwavelength resolved scattered light images. The radial segregation is noted in the spatially resolved millimeter/radio continuum "colors."

2. Additional evidence for the inward migration of particles due to radial drift is available in the form of a steep drop in the dust-to-gas ratio, observationally manifested as a sharp-edged continuum profile and a substantial size discrepancy between resolved tracers of gas and millimeter/centimeter particles.

3. The population of "transition disks" is characterized by a ring-like dust geometry, with larger particles (observed in the millimeter/centimeter continuum) concentrated in a narrow annulus outside a central, depleted cavity. In the specific examples studied in detail so far, gas and smaller particles extend into the cavity and out to larger radii. The physical interpretation of these structures is related to the presence of a radial maximum in the gas pressure profile, which effectively traps large particles.

4. A subset of the transition disk population also exhibits a variety of substructures, in the forms of azimuthal asymmetries, spiral patterns, and vertical warps. The current thinking is that these massive, still-accreting systems represent young (giant) planetary systems during their formation epoch.

Additional Reading: The sequence of reviews on the evolution of disk solids by Beckwith et al. (2000), Natta et al. (2007), and Testi et al. (2014); the more general review on disk evolution by Alexander (2008); and the recent overviews of disk dispersal and transition disks by Alexander et al. (2014) and Espaillat et al. (2014).

7. FUTURE DIRECTIONS

The intentions of this review were to highlight some of the fundamental aspects of this field and their key applications, and to hopefully serve as a pedagogical resource (or starting point) for those interested in joining the related research efforts. The past few years have seen dramatic advances in the observational study of circumstellar disks, and particularly their connections to the formation epoch for planetary systems. It is not a stretch to argue that at this stage the subject could be better characterized as "observational planet formation." The field is poised for substantial continued development, owing particularly to the capabilities of the nearly completed ALMA project. Given that promise, there seems little doubt that the landscape of disk research will look significantly different in the next decade. Although it is difficult to predict that future, the first steps along the path toward it are now relatively clear.

Prominent among these is an effort to sort out some of the basic demographics of disk properties, and thereby the key factors that impact planet formation efficiencies. § 4 introduced the early efforts along these lines, pointing out the preliminary indications that disk masses (and thereby the likelihood for planet formation) depend on the stellar host mass (§ 4.1), multiplicity (§ 4.2), and environment (§ 4.3). But, so far, the limitations on the sizes and properties of samples has stifled further inquiry along these lines. That will change with ALMA; several survey projects are underway, and more will surely follow. There are many opportunities to address some fundamental questions in the field with creative explorations of the data available from such surveys. How does the disk mass distribution evolve? What are the interdependences between and evolutionary behavior of the demographic trends that have been noted so far? What accounts for the tremendous scatter around these trends? How does the gas reservoir, as traced by key spectral line ratios (e.g., Williams & Best 2014), behave with respect to the solids? How are these simple, compound diagnostic relations tied to more detailed, elemental (i.e., resolved) measurements?

The last of these questions connects back to the fundamental goal of constraining disk density structures (§ 5). In the near term, progress toward that goal from continuum data alone is a major challenge. Intrinsic uncertainties in the opacities of disk solids (§ 5.3), coupled with the complex processes of growth and migration that modify their sizes and spatial distributions (§ 6.1), make a robust and quantitative characterization of the densities prohibitive without additional information. One way around this impasse is to forge closer links to the wealth of spectral line measurements available from ALMA observations. At this stage, developing a robust forward-modeling approach to "fit" a large and complex union of datasets with an ever-expanding (and not well-justified) set of (pseudo) physical parameters is intractable. Instead, emphasis should be placed on identifying and characterizing patterns among resolved, multi-tracer diagnostics. For spectral line data, these might include the locations of condensation fronts (Qi et al. 2011, 2013; Mathews et al. 2013), molecular abundance patterns (e.g., Öberg et al. 2010, 2011; see Dutrey et al. 2014), or constraints on the vertical temperature distribution (Dartois et al. 2003; Rosenfeld et al. 2013a; de Gregorio-Monsalvo et al. 2013). How do these and other measurements behave as a function of basic demographic properties? How are they related to the resolved morphologies of the continuum emission?

An important complementary approach involves building on the patterns already emerging from resolved continuum datasets, and associating these with the theoretical predictions from models of the evolution of disk solids (§ 6.1). Does the tentative correlation between continuum luminosities and sizes (§ 5.2) hold up for larger and different samples, and does it depend on other demographic properties? How is the radial variation in millimeter/radio "color" or the location and shape of the outer edge of the continuum emission (§ 6.1) connected to factors like the evolutionary state, stellar host, or the structure of the gas reservoir? And, most pressing, can high angular resolution continuum measurements find and characterize evidence for the small-scale substructure presumed to be responsible for mitigating high radial drift rates, and thereby preserving large particles in the outer disk? The stunning recent ALMA image of the canonical HL Tau disk, shown in Figure 20, hints that a major conceptual evolution related to this last question is underway (ALMA Partnership et al. 2015).

Substructure observed in these disks will be especially important in developing a comprehensive model for the formation

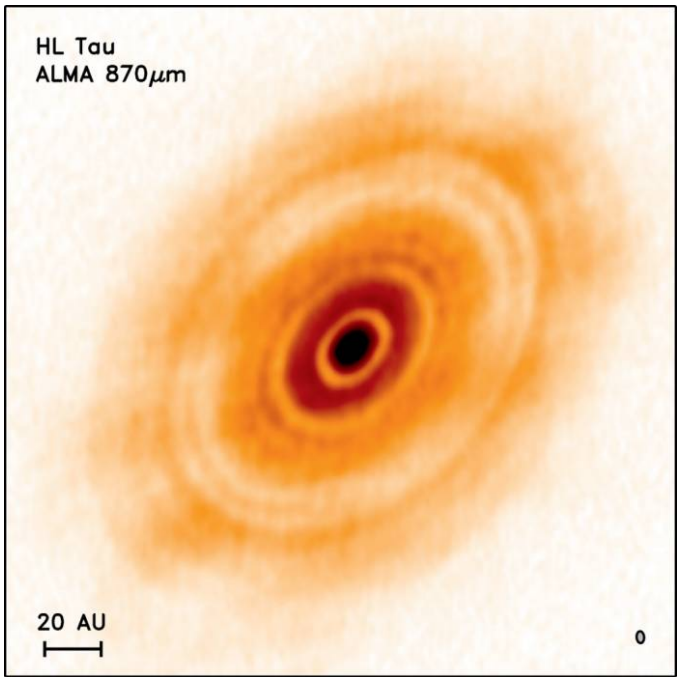

FIG. 20.—HL Tau disk observed at high angular resolution (0.″05, or ~7 AU) in the 870 μm continuum. A series of concentric rings are presumably responsible for slowing or halting radial drift and are likely the active, telltale signatures of planetary system formation (ALMA Partnership et al. 2015). See the electronic edition of the *PASP* for a color version of this figure.

and early evolution of planetary systems. If HL Tau is any indication, observations with ALMA may find the general disk population riddled with young multiplanet systems carving out concentric, apparently resonant, gaps in their natal material. Or perhaps the larger scale asymmetries identified for many transition disks (§ 6.2) indicate that a less-orderly phenomenology will be more common. In any case, the underlying issue on this topic is finding ways to quantitatively link the small-scale features that are observed to the physical properties of associated planets and the mechanics of the disk-planet interactions. How can multitracer measurements of (gas and dust) substructure be optimally combined to robustly estimate a perturber mass and differentiate it from the effects of viscous turbulence? What level of diversity in scales and amplitudes are present in this substructure, and how does it vary as a function of the evolutionary state or basic demographic properties? How can disk observations be exploited to optimize searches for young planets? And, when successful, what can the combined measurements of planets and their birth reservoirs say about the processes of planetary formation, migration, and accretion?

In the larger context of piecing together our cosmic origins, these are deep, pressing questions. It is remarkable to think that the key technological resources needed to address these questions are now available and that answers (and new questions) are sure to follow.

I am very grateful to David Wilner and Til Birnstiel for many helpful discussions and assistance related to the organization and content of this review. The presentation also greatly benefitted from the insightful comments and suggestions kindly offered by Megan Ansdell, Xuening Bai, John Carpenter, Antonella Natta, Karin Öberg, Chunhua Qi, Anjali Tripathi, Jonathan Williams, and an anonymous reviewer. I would especially like to thank Til Birnstiel, Kate Follette, Antonio Garufi, Rita Mann, Laura Pérez, and Karl Stapefeldt for their willingness to share data to help make some of the figures, as well as John Debes, Carol Grady, Christophe Pinte, Massimo Robberto, and Glenn Schneider for kindly offering permission to reproduce some of their published figures.

REFERENCES

Abt, H. A., & Levy, S. G. 1976, ApJS, 30, 273
Acke, B., van den Ancker, M. E., Dullemond, C. P., van Boekel, R., & Waters, L. B. F. M. 2004, A&A, 422, 621
Adachi, I., Hayashi, C., & Nakazawa, K. 1976, Prog. Theor. Phys., 56, 1756
Adams, F. C., Emerson, J. P., & Fuller, G. A. 1990, ApJ, 357, 606
Adams, F. C., Lada, C. J., & Shu, F. H. 1987, ApJ, 312, 788
———. 1988, ApJ, 326, 865
Adams, F. C., Proszkow, E. M., Fatuzzo, M., & Myers, P. C. 2006, ApJ, 641, 504
Adams, F. C., & Shu, F. H. 1986, ApJ, 308, 836
Akeson, R. L., Ciardi, D. R., van Belle, G. T., & Creech-Eakman, M. J. 2002, ApJ, 566, 1124
Akeson, R. L., & Jensen, E. L. N. 2014, ApJ, 784, 62
Akeson, R. L., Rice, W. K. M., Boden, A. F., Sargent, A. I., Carpenter, J. M., & Bryden, G. 2007, ApJ, 670, 1240
Alexander, R. 2008, NewA Rev., 52, 60
Alexander, R., Pascucci, I., Andrews, S., Armitage, P., & Cieza, L. 2014, in Protostars and Planets VI, ed. H. Beuther, et al. (Tucson: Univ. Arizona Press), 475
Alexander, R. D., & Armitage, P. J. 2007, MNRAS, 375, 500
———. 2009, ApJ, 704, 989
Alexander, R. D., Clarke, C. J., & Pringle, J. E. 2006a, MNRAS, 369, 216
———. 2006b, MNRAS, 369, 229
Alfvén, H., & Arrhenius, G. 1970, Ap&SS, 8, 338
Alibert, Y., Mordasini, C., & Benz, W. 2011, A&A, 526, A 63
ALMA Partnership, Brogan, C. L., et al. 2015, ApJ, 808, L3
Andre, P., & Montmerle, T. 1994, ApJ, 420, 837
Andrews, S. M., Czekala, I., Wilner, D. J., Espaillat, C., Dullemond, C. P., & Hughes, A. M. 2010a, ApJ, 710, 462
Andrews, S. M., Rosenfeld, K. A., Kraus, A. L., & Wilner, D. J. 2013, ApJ, 771, 129
Andrews, S. M., & Williams, J. P. 2005, ApJ, 631, 1134
———. 2007a, ApJ, 671, 1800

———. 2007b, ApJ, 659, 705
Andrews, S. M., Wilner, D. J., Espaillat, C., Hughes, A. M., Dullemond, C. P., McClure, M. K., Qi, C., & Brown, J. M. 2011, ApJ, 732, 42
Andrews, S. M., Wilner, D. J., Hughes, A. M., Qi, C., & Dullemond, C. P. 2009, ApJ, 700, 1502
———. 2010b, ApJ, 723, 1241
Andrews, S. M., et al. 2012, ApJ, 744, 162
———. 2014, ApJ, 787, 148
Ansdell, M., Williams, J. P., & Cieza, L. A. 2015, ApJ, 806, 221
Artymowicz, P., & Lubow, S. H. 1994, ApJ, 421, 651
———. 1996, ApJ, 467, L 77
Augereau, J. C., Lagrange, A. M., Mouillet, D., & Ménard, F. 2001, A&A, 365, 78
Avenhaus, H., Quanz, S. P., Schmid, H. M., Meyer, M. R., Garufi, A., Wolf, S., & Dominik, C. 2014, ApJ, 781, 87
Bai, X.-N. 2015, ApJ, 798, 84
Bai, X.-N., & Stone, J. M. 2013, ApJ, 769, 76
———. 2014, ApJ, 796, 31
Bally, J., O'Dell, C. R., & McCaughrean, M. J. 2000, AJ, 119, 2919
Bally, J., Sutherland, R. S., Devine, D., & Johnstone, D. 1998a, AJ, 116, 293
Bally, J., Testi, L., Sargent, A., & Carlstrom, J. 1998b, AJ, 116, 854
Banzatti, A., Testi, L., Isella, A., Natta, A., Neri, R., & Wilner, D. J. 2011, A&A, 525, A 12
Barge, P., & Sommeria, J. 1995, A&A, 295, L 1
Bastien, P. 1982, A&AS, 48, 153
Bastien, P., & Menard, F. 1988, ApJ, 326, 334
———. 1990, ApJ, 364, 232
Bate, M. R. 2000, MNRAS, 314, 33
Bate, M. R., & Bonnell, I. A. 1997, MNRAS, 285, 33
Beckwith, S., Skrutskie, M. F., Zuckerman, B., & Dyck, H. M. 1984, ApJ, 287, 793
Beckwith, S. V. W. 1999, in The Origin of Stars and Planetary Systems, ed. C. J. Lada, & N. D. Kylafis (NATO ASI Ser. C, 540; Dordrecht: Springer), 579
Beckwith, S. V. W., Henning, T., & Nakagawa, Y. 2000, in Protostars and Planets IV, eds. V. Mannings, A. P. Boss, & S. S. Russell (Tucson: Univ. Arizona Press), 533
Beckwith, S. V. W., & Sargent, A. I. 1991, ApJ, 381, 250
Beckwith, S. V. W., Sargent, A. I., Chini, R. S., & Guesten, R. 1990, AJ, 99, 924
Bell, K. R. 1999, ApJ, 526, 411
Bell, K. R., Cassen, P. M., Klahr, H. H., & Henning, T. 1997, ApJ, 486, 372
Benz, W., Ida, S., Alibert, Y., Lin, D., & Mordasini, C. 2014, in Protostars and Planets VI, ed. H. Beuther, et al. (Tucson: Univ. Arizona Press), 691
Bertout, C., Basri, G., & Bouvier, J. 1988, ApJ, 330, 350
Biller, B. A., et al. 2014, ApJ, 792, L 22
Birnstiel, T., & Andrews, S. M. 2014, ApJ, 780, 153
Birnstiel, T., Dullemond, C. P., & Brauer, F. 2009, A&A, 503, L 5
Birnstiel, T., Dullemond, C. P., & Brauer, F. 2010, A&A, 513, A 79
Birnstiel, T., Dullemond, C. P., & Pinilla, P. 2013, A&A, 550, L 8
Birnstiel, T., Klahr, H., & Ercolano, B. 2012, A&A, 539, A 148
Bjorkman, J. E., & Wood, K. 2001, ApJ, 554, 615
Blandford, R. D., & Payne, D. G. 1982, MNRAS, 199, 883
Blum, J., & Wurm, G. 2008, ARA&A, 46, 21
Boehler, Y., Dutrey, A., Guilloteau, S., & Piétu, V. 2013, MNRAS, 431, 1573
Boffin, H. M. J., Watkins, S. J., Bhattal, A. S., Francis, N., & Whitworth, A. P. 1998, MNRAS, 300, 1189
Bohren, C.F., & Huffman, D. R. 1983, Absorption and Scattering of Light by Small Particles (Weinheim: Wiley)
Bonavita, M., & Desidera, S. 2007, A&A, 468, 721
Boss, A. P. 2011, ApJ, 731, 74
Bouwman, J., Meeus, G., de Koter, A., Hony, S., Dominik, C., & Waters, L. B. F. M. 2001, A&A, 375, 950
Bowler, B. P., et al. 2010, ApJ, 709, 396
Brauer, F., Dullemond, C. P., & Henning, T. 2008, A&A, 480, 859
Brauer, F., Dullemond, C. P., Johansen, A., Henning, Th., Klahr, H., & Natta, A. 2007, A&A, 469, 1169
Breslau, A., Steinhausen, M., Vincke, K., & Pfalzner, S. 2014, A&A, 565, A 130
Brown, J. M., Blake, G. A., Qi, C., Dullemond, C. P., & Wilner, D. J. 2008, ApJ, 675, L 109
Brown, J. M., Blake, G. A., Qi, C., Dullemond, C. P., Wilner, D. J., & Williams, J. P. 2009, ApJ, 704, 496
Brown, J. M., Rosenfeld, K. A., Andrews, S. M., Wilner, D. J., & van Dishoeck, E. F. 2012, ApJ, 758, L 30
Brown, J. M., et al. 2007, ApJ, 664, L 107
Bruderer, S., van der Marel, N., van Dishoeck, E. F., & van Kempen, T. A. 2014, A&A, 562, A 26
Bruggeman, D. A. G. 1935, Annalen der Physik, 416, 636
Brush, S. G. 1978a, J. Hist. of Astron., 9, 1
———. 1978b, J. Hist. of Astron., 9, 77
———. 1981, in Space Science Comes of Age: Perspectives in the History of the Space Sciences, ed. P. A. Hanle, & V. D. Chamberlain (Washington: Smithsonian Institute Press), 78
———. 1990, Rev. Mod. Phys., 62, 43
Bryden, G., Chen, X., Lin, D. N. C., Nelson, R. P., & Papaloizou, J. C. B. 1999, ApJ, 514, 344
Burrows, C. J., et al. 1996, ApJ, 473, 437
Cabrit, S., Edwards, S., Strom, S. E., & Strom, K. M. 1990, ApJ, 354, 687
Calvet, N., D'Alessio, P., Hartmann, L., Wilner, D., Walsh, A., & Sitko, M. 2002, ApJ, 568, 1008
Calvet, N., Magris, G. C., Patino, A., & D'Alessio, P. 1992, Rev. Mex. AA, 24, 27
Calvet, N., Patino, A., Magris, G. C., & D'Alessio, P. 1991, ApJ, 380, 617
Calvet, N., et al. 2005, ApJ, 630, L 185
Cameron, A. G. W. 1962, Icarus, 1, 13
———. 1988, ARA&A, 26, 441
Canovas, H., Ménard, F., Hales, A., Jordán, A., Schreiber, M. R., Casassus, S., Gledhill, T. M., & Pinte, C. 2013, A&A, 556, A 123
Canovas, H., et al. 2015, ApJ, 805, 21
Cardelli, J. A., Clayton, G. C., & Mathis, J. S. 1989, ApJ, 345, 245
Carpenter, J. M. 2002, AJ, 124, 1593
Carpenter, J. M., Ricci, L., & Isella, A. 2014, ApJ, 787, 42
Casassus, S., et al. 2013, Nature, 493, 191
Cassen, P., & Moosman, A. 1981, Icarus, 48, 353
Cassen, P., & Summers, A. 1983, Icarus, 53, 26
Chamberlin, T. C. 1900, J. Geology, 8, 58
Chiang, E. I., & Goldreich, P. 1997, ApJ, 490, 368
———. 1999, ApJ, 519, 279

Chiang, E. I., Joung, M. K., Creech-Eakman, M. J., Qi, C., Kessler, J. E., Blake, G. A., & van Dishoeck, E. F. 2001, ApJ, 547, 1077
Churchwell, E., Felli, M., Wood, D. O. S., & Massi, M. 1987, ApJ, 321, 516
Cieza, L. A., Schreiber, M. R., Romero, G. A., Williams, J. P., Rebassa-Mansergas, A., & Merín, B. 2012, ApJ, 750, 157
Cieza, L. A., Swift, J. J., Mathews, G. S., & Williams, J. P. 2008, ApJ, 686, L 115
Cieza, L., et al. 2007, ApJ, 667, 308
———. 2009, ApJ, 696, L 84
Clampin, M., et al. 2003, AJ, 126, 385
Clarke, C. J., Gendrin, A., & Sotomayor, M. 2001, MNRAS, 328, 485
Clarke, C. J., & Pringle, J. E. 1993, MNRAS, 261, 190
Close, L. M., et al. 1998, ApJ, 499, 883
Cody, A. M., et al. 2014, AJ, 147, 82
Cohen, M. 1973, MNRAS, 164, 395
———. 1980, MNRAS, 191, 499
———. 1983, ApJ, 270, L 69
Cohen, M., Harvey, P. M., & Schwartz, R. D. 1985, ApJ, 296, 633
Cohen, M., & Kuhi, L. V. 1979, ApJS, 41, 743
Cohen, M., & Witteborn, F. C. 1985, ApJ, 294, 345
Cotera, A. S., et al. 2001, ApJ, 556, 958
Creech-Eakman, M. J., Chiang, E. I., Joung, R. M. K., Blake, G. A., & van Dishoeck, E. F. 2002, A&A, 385, 546
Crida, A., & Morbidelli, A. 2007, MNRAS, 377, 1324
Cuzzi, J. N., Dobrovolskis, A. R., & Champney, J. M. 1993, Icarus, 106, 102
D'Alessio, P., Calvet, N., & Hartmann, L. 2001, ApJ, 553, 321
D'Alessio, P., Calvet, N., Hartmann, L., Franco-Hernández, R., & Servín, H. 2006, ApJ, 638, 314
D'Alessio, P., Calvet, N., Hartmann, L., Lizano, S., & Cantó, J. 1999, ApJ, 527, 893
D'Alessio, P., Canto, J., Calvet, N., & Lizano, S. 1998, ApJ, 500, 411
D'Alessio, P., et al. 2005, ApJ, 621, 461
Dartois, E., Dutrey, A., & Guilloteau, S. 2003, A&A, 399, 773
Davis, S. S. 2005, ApJ, 627, L 153
de Gregorio-Monsalvo, I., Ménard, F., Dent, W.et al. 2013, A&A, 557, A 133
Debes, J. H., Jang-Condell, H., Weinberger, A. J., Roberge, A., & Schneider, G. 2013, ApJ, 771, 45
Debes, J. H., Weinberger, A. J., & Schneider, G. 2008, ApJ, 673, L 191
Desch, S. J. 2007, ApJ, 671, 878
Desidera, S., & Barbieri, M. 2007, A&A, 462, 345
Dipierro, G., Lodato, G., Testi, L., & de Gregorio Monsalvo, I. 2014, MNRAS, 444, 1919
Dipierro, G., Pinilla, P., Lodato, G., & Testi, L. 2015, MNRAS, 451, 974
Dodson-Robinson, S. E., & Salyk, C. 2011, ApJ, 738, 131
Dohnanyi, J. S. 1969, J. Geophys. Res., 74, 2531
Dominik, C., & Dullemond, C. P. 2008, A&A, 491, 663
Dominik, C., Dullemond, C. P., Waters, L. B. F. M., & Walch, S. 2003, A&A, 398, 607
Dominik, C., & Tielens, A. G. G. M. 1997, ApJ, 480, 647
Dong, R., et al. 2012, ApJ, 750, 161
Dorschner, J., Begemann, B., Henning, T., Jaeger, C., & Mutschke, H. 1995, A&A, 300, 503
Draine, B. T. 2006, ApJ, 636, 1114
Draine, B. T., & Flatau, P. J. 1994, J Opt. Soc. Am. A, 11, 1491
Draine, B. T., & Lee, H. M. 1984, ApJ, 285, 89
Dubrulle, B., Morfill, G., & Sterzik, M. 1995, Icarus, 114, 237
Duchêne, G., & Kraus, A. 2013, ARA&A, 51, 269
Duchêne, G., McCabe, C., Ghez, A. M., & Macintosh, B. A. 2004, ApJ, 606, 969
Duchêne, G., Ménard, F., Stapelfeldt, K., & Duvert, G. 2003, A&A, 400, 559
Duchêne, G., et al. 2010, ApJ, 712, 112
Dullemond, C. P., & Dominik, C. 2004a, A&A, 417, 159
———. 2004b, A&A, 421, 1075
———. 2005, A&A, 434, 971
Dullemond, C. P., Dominik, C., & Natta, A. 2001, ApJ, 560, 957
Dullemond, C. P., Hollenbach, D., Kamp, I., & D'Alessio, P. 2007, in Protostars and Planets V, ed. B. Reipurth, D. Jewitt, & K. Keil (Tucson: Univ. Arizona Press), 555
Dullemond, C. P., & Monnier, J. D. 2010, ARA&A, 48, 205
Dullemond, C. P., van Zadelhoff, G. J., & Natta, A. 2002, A&A, 389, 464
Duquennoy, A., & Mayor, M. 1991, A&A, 248, 485
Dutrey, A., Guilloteau, S., Duvert, G., Prato, L., Simon, M., Schuster, K., & Menard, F. 1996, A&A, 309, 493
Dutrey, A., Guilloteau, S., & Simon, M. 1994, A&A, 286, 149
Dutrey, A., et al. 2014, in Protostars and Planets VI, ed. H. Beuther, et al. (Tucson: Univ. Arizona Press), 317
Dzyurkevich, N., Turner, N. J., Henning, T., & Kley, W. 2013, ApJ, 765, 114
Edgeworth, K. E. 1949, MNRAS, 109, 600
Edwards, S., Cabrit, S., Strom, S. E., Heyer, I., Strom, K. M., & Anderson, E. 1987, ApJ, 321, 473
Eisner, J. A., & Carpenter, J. M. 2003, ApJ, 598, 1341
———. 2006, ApJ, 641, 1162
Eisner, J. A., Plambeck, R. L., Carpenter, J. M., Corder, S. A., Qi, C., & Wilner, D. 2008, ApJ, 683, 304
Elsasser, H., & Staude, H. J. 1978, A&A, 70, L 3
Enoch, M. L., et al. 2006, ApJ, 638, 293
Ercolano, B., Clarke, C. J., & Drake, J. J. 2009, ApJ, 699, 1639
Ercolano, B., Drake, J. J., Raymond, J. C., & Clarke, C. C. 2008, ApJ, 688, 398
Espaillat, C., Calvet, N., D'Alessio, P., Hernández, J., Qi, C., Hartmann, L., Furlan, E., & Watson, D. M. 2007, ApJ, 670, L 135
Espaillat, C., Calvet, N., Luhman, K. L., Muzerolle, J., & D'Alessio, P. 2008, ApJ, 682, L 125
Espaillat, C., Furlan, E., D'Alessio, P., Sargent, B., Nagel, E., Calvet, N., Watson, D. M., & Muzerolle, J. 2011, ApJ, 728, 49
Espaillat, C., et al. 2010, ApJ, 717, 441
———. 2012, ApJ, 747, 103
———. 2014, in Protostars and Planets VI, ed. H. Beuther, et al. (Tucson: Univ. Arizona Press), 497
Evans, N. J., II, et al. 2009, ApJS, 181, 321
Fang, M., van Boekel, R., Wang, W., Carmona, A., Sicilia-Aguilar, A., & Henning, Th. 2009, A&A, 504, 461
Finkbeiner, D. P., Davis, M., & Schlegel, D. J. 1999, ApJ, 524, 867
Fischer, D. A., Howard, A. W., Laughlin, G. P., Macintosh, B., Mahadevan, S., Sahlmann, J., & Yee, J. C. 2014, in Protostars and Planets VI, ed. H. Beuther, et al. (Tucson: Univ. Arizona Press), 715
Flaherty, K. M., & Muzerolle, J. 2010, ApJ, 719, 1733

Flaherty, K. M., Muzerolle, J., Rieke, G., Gutermuth, R., Balog, Z., Herbst, W., & Megeath, S. T. 2013, AJ, 145, 66
———. 2012, ApJ, 748, 71
Flock, M., et al. 2015, A&A, 574, A 68
Follette, K. B., et al. 2013, ApJ, 767, 10
Font, A. S., McCarthy, I. G., Johnstone, D., & Ballantyne, D. R. 2004, ApJ, 607, 890
Forrest, W. J., et al. 2004, ApJS, 154, 443
Fukagawa, M., Tamura, M., Itoh, Y., Kudo, T., Imaeda, Y., Oasa, Y., Hayashi, S. S., & Hayashi, M. 2006, ApJ, 636, L 153
Fukagawa, M., et al. 2004, ApJ, 605, L 53
———. 2013, PASJ, 65, L 14
Furlan, E., et al. 2009, ApJ, 703, 1964
———. 2011, ApJS, 195, 3
Garufi, A., Quanz, S. P., Schmid, H. M., Avenhaus, H., Buenzil, E., & Wolf, S. 2014, A&A, 568, A 40
Garufi, A., et al. 2013, A&A, 560, A 105
Geers, V. C., van Dishoeck, E. F., Visser, R., Pontoppidan, K. M., Augereau, J.-C., Habart, E., & Lagrange, A. M. 2007, A&A, 476, 279
Geers, V. C., et al. 2006, A&A, 459, 545
Geisel, S. L. 1970, ApJ, 161, L 105
Ghez, A. M., Neugebauer, G., & Matthews, K. 1993, AJ, 106, 2005
Gillett, F. C., & Stein, W. A. 1971, ApJ, 164, 77
Glauser, A. M., Ménard, F., Pinte, C., Duchêne, M., Güdel, M., Monin, J.-L., & Padgett, D. L. 2008, A&A, 485, 531
Goldreich, P., & Tremaine, S. 1980, ApJ, 241, 425
Goldsmith, P. F., Bergin, E. A., & Lis, D. C. 1997, ApJ, 491, 615
Gorti, U., Dullemond, C. P., & Hollenbach, D. 2009, ApJ, 705, 1237
Gorti, U., & Hollenbach, D. 2009, ApJ, 690, 1539
Gorti, U., Hollenbach, D., & Dullemond, C. P. 2015, ApJ, 804, 29
Grady, C. A., Woodgate, B., Bruhweiler, F. C., Boggess, A., Plait, P., Lindler, D. J., Clampin, M., & Kalas, P. 1999, ApJ, 523, L 151
Grady, C. A., et al. 2000, ApJ, 544, 895
———. 2007, ApJ, 665, 1391
———. 2013, ApJ, 762, 48
Gräfe, C., Wolf, S., Guilloteau, S., Dutrey, A., Stapelfeldt, K. R., Pontoppidan, K. M., & Sauter, J. 2013, A&A, 553, A 69
Grasdalen, G. L., Strom, S. E., Strom, K. M., Capps, R. W., Thompson, D., & Castelaz, M. 1984, ApJ, 283, L 57
Greaves, J. S., & Rice, W. K. M. 2010, MNRAS, 407, 1981
Guilloteau, S., Dutrey, A., Piétu, V., & Boehler, Y. 2011, A&A, 529, A 105
Güttler, C., Blum, J., Zsom, A., Ormel, C. W., & Dullemond, C. P. 2010, A&A, 513, A 56
Habart, E., Natta, A., & Krügel, E. 2004, A&A, 427, 179
Haisch, K. E., Jr., Lada, E. A., & Lada, C. J. 2001, ApJ, 553, L 153
Hamidouche, M., Looney, L. W., & Mundy, L. G. 2006, ApJ, 651, 321
Harris, R. J., Andrews, S. M., Wilner, D. J., & Kraus, A. L. 2012, ApJ, 751, 115
Harris, S., Clegg, P., & Hughes, J. 1988, MNRAS, 235, 441
Hartmann, L. 2008, Accretion Processes in Star Formation (2nd ed.; Cambridge: Cambridge Univ. Press), chap. 8
Hartmann, L., Calvet, N., Gullbring, E., & D'Alessio, P. 1998, ApJ, 495, 385
Hartmann, L., D'Alessio, P., Calvet, N., & Muzerolle, J. 2006, ApJ, 648, 484
Hartmann, L., & Kenyon, S. J. 1985, ApJ, 299, 462
Hashimoto, J., et al. 2011, ApJ, 729, L 17
———. 2012, ApJ, 758, L 19
Hayashi, C. 1981, Prog. Theor. Phys. Suppl., 70, 35
Hayashi, M., Ohashi, N., & Miyama, S. M. 1993, ApJ, 418, L 71
Henney, W. J., & O'Dell, C. R. 1999, AJ, 118, 2350
Henning, T., Begemann, B., Mutschke, H., & Dorschner, J. 1995, A&AS, 112, 143
Henning, T., & Stognienko, R. 1996, A&A, 311, 291
Henning, T., & Thamm, E. 1994, Ap&SS, 212, 215
Herbig, G. H. 1960, ApJS, 4, 337
———. 1962, Adv. Astron. Astrophys., 1, 47
Hernández, J., Hartmann, L., Calvet, N., Jeffries, R. D., Gutermuth, R., Muzerolle, J., & Stauffer, J. 2008, ApJ, 686, 1195
Hernández, J., et al. 2007, ApJ, 662, 1067
Hildebrand, R. H. 1983, QJRAS, 24, 267
Hillenbrand, L. A. 2008, Phys. Scr., T130, 014024
Hillenbrand, L. A., et al. 2008, ApJ, 677, 630
Hinkley, S., et al. 2009, ApJ, 701, 804
Hogerheijde, M. R., Jayawardhana, R., Johnstone, D., Blake, G. A., & Kessler, J. E. 2002, AJ, 124, 3387
Hollenbach, D., Johnstone, D., Lizano, S., & Shu, F. 1994, ApJ, 428, 654
Honda, M., Kataza, H., Okamoto, Y. K., Miyata, T., Yamashita, T., Sako, S., Tabuko, S., & Onaka, T. 2003, ApJ, 585, L 59
Howard, A. W. 2013, Science, 340, 572
Hoyle, F. 1960, QJRAS, 1, 28
Hubickyj, O., Bodenheimer, P., & Lissauer, J. J. 2005, Icarus, 179, 415
Huélamo, N., de Gregorio-Monsalvo, I., Macias, E., Pinte, C., Ireland, M., Tuthill, P., & Lacour, S. 2015, A&A, 575, L 5
Huélamo, N., Lacour, S., Tuthill, P., Ireland, M., Kraus, A., & Chauvin, G. 2011, A&A, 528, L 7
Hueso, R., & Guillot, T. 2005, A&A, 442, 703
Hughes, A. M., Hull, C. L. H., Wilner, D. J., & Plambeck, R. L. 2013, AJ, 145, 115
Hughes, A. M., Wilner, D. J., Calvet, N., D'Alessio, P., Claussen, M. J., & Hogerheijde, M. R. 2007, ApJ, 664, 536
Hughes, A. M., Wilner, D. J., Cho, J., Marrone, D. P., Lazarian, A., Andrews, S. M., & Rao, R. 2009a, ApJ, 704, 1204
Hughes, A. M., Wilner, D. J., Qi, C., & Hogerheijde, M. R. 2008, ApJ, 678, 1119
Hughes, A. M., et al. 2009b, ApJ, 698, 131
Ida, S., & Lin, D. N. C. 2005, ApJ, 626, 1045
Ingleby, L., Calvet, N., Hernández, J., Hartmann, L., Briceno, C., Miller, J., Espaillat, C., & McClure, M. 2014, ApJ, 790, 47
Ireland, M. J., & Kraus, A. L. 2008, ApJ, 678, L 59
Isella, A., Carpenter, J. M., & Sargent, A. I. 2009, ApJ, 701, 260
———. 2010a, ApJ, 714, 1746
Isella, A., Natta, A., Wilner, D., Carpenter, J. M., & Testi, L. 2010b, ApJ, 725, 1735
Isella, A., Pérez, L. M., Carpenter, J. M., Ricci, L., Andrews, S., & Rosenfeld, K. 2013, ApJ, 775, 30
Isella, A., Testi, L., Natta, A., Neri, R., Wilner, D., & Qi, C. 2007, A&A, 469, 213
Jacquet, E., Gounelle, M., & Fromang, S. 2012, Icarus, 220, 162
Jaeger, C., Molster, F. J., Dorschner, J., Henning, Th., Mutschke, H., & Waters, L. B. F. M. 1998, A&A, 339, 904
Jaeger, C., Mutschke, H., Begemann, B., Dorschner, J., & Henning, T. 1994, A&A, 292, 641

Jang-Condell, H., & Boss, A. P. 2007, ApJ, 659, L 169
Jensen, E. L. N., & Akeson, R. 2014, Nature, 511, 567
Jensen, E. L. N., & Akeson, R. L. 2003, ApJ, 584, 875
Jensen, E. L. N., Mathieu, R. D., Donar, A. X., & Dullighan, A. 2004, ApJ, 600, 789
Jensen, E. L. N., Mathieu, R. D., & Fuller, G. A. 1994, ApJ, 429, L 29
———. 1996, ApJ, 458, 312
Johansen, A., Youdin, A., & Klahr, H. 2009, ApJ, 697, 1269
Johnson, J. A., Aller, K. M., Howard, A. W., & Crepp, J. R. 2010, PASP, 122, 905
Johnson, J. A., Butler, R. P., Marcy, G. W., Fischer, D. A., Vogt, S. S., Wright, J. T., & Peek, K. M. G. 2007, ApJ, 670, 833
Johnstone, D., Hollenbach, D., & Bally, J. 1998, ApJ, 499, 758
Joy, A. H. 1945, ApJ, 102, 168
———. 1949, ApJ, 110, 424
Juhasz, A., Benisty, M., Pohl, A., Dullemond, C., Dominik, C., & PaardekooperS.-J. 2015, MNRAS, 451, 1147
Kant, I. 1755, Allgemeine Naturgeschichte und Theorie des Himmels
Kataoka, A., Okuzumi, S., Tanaka, H., & Nomura, H. 2014, A&A, 568, A 42
Keene, J., & Masson, C. R. 1990, ApJ, 355, 635
Keller, L. D., et al. 2008, ApJ, 684, 411
Kennedy, G. M., & Kenyon, S. J. 2008, ApJ, 673, 502
Kenyon, S. J., & Bromley, B. C. 2006, AJ, 131, 1837
Kenyon, S. J., & Hartmann, L. 1987, ApJ, 323, 714
Kenyon, S. J., & Webbink, R. F. 1984, ApJ, 279, 252
Kessler-Silacci, J., et al. 2006, ApJ, 639, 275
Kessler-Silacci, J. E., Hillenbrand, L. A., Blake, G. A., & Meyer, M. R. 2005, ApJ, 622, 404
Kimura, H., Kolokolova, L., & Mann, I. 2003, A&A, 407, L 5
Kitamura, Y., Momose, M., Yokogawa, S., Kawabe, R., Tamura, M., & Ida, S. 2002, ApJ, 581, 357
Klahr, H. H., & Henning, T. 1997, Icarus, 128, 213
Klein, R., Apai, D., Pascucci, I., Henning, T., & Waters, L. B. F. M. 2003, ApJ, 593, L 57
Kley, W. 1999, MNRAS, 303, 696
Kley, W., & Dirksen, G. 2006, A&A, 447, 369
Kley, W., & Nelson, R. P. 2012, ARA&A, 50, 211
Kley, W., Papaloizou, J. C. B., & Ogilvie, G. I. 2008, A&A, 487, 671
Kobayashi, H., & Ida, S. 2001, Icarus, 153, 416
Koerner, D. W., Chandler, C. J., & Sargent, A. I. 1995, ApJ, 452, L 69
Koerner, D. W., Sargent, A. I., & Beckwith, S. V. W. 1993, Icarus, 106, 2
Kokubo, E., & Ida, S. 2002, ApJ, 581, 666
Kokubo, E., Kominami, J., & Ida, S. 2006, ApJ, 642, 1131
Konigl, A. 1989, ApJ, 342, 208
Kornet, K., Wolf, S., & Różyczka, M. 2006, A&A, 458, 661
Korycansky, D. G., & Papaloizou, J. C. B. 1995, MNRAS, 274, 85
Kóspál, Á., et al. 2012, ApJS, 201, 11
Kozasa, T., Blum, J., & Mukai, T. 1992, A&A, 263, 423
Kraus, A. L., & Ireland, M. J. 2012, ApJ, 745, 5
Kraus, A. L., Ireland, M. J., Hillenbrand, L. A., & Martinache, F. 2012, ApJ, 745, 19
Kraus, A. L., Ireland, M. J., Martinache, F., & Hillenbrand, L. A. 2011, ApJ, 731, 8
Kretke, K. A., & Lin, D. N. C. 2007, ApJ, 664, L 55
Krijt, S., Ormel, C. W., Dominik, C., & Tielens, A. G. G. M. 2015, A&A, 574, A 83
Krist, J. E., Stapelfeldt, K. R., Ménard, F., Padgett, D. L., & Burrows, C. J. 2000, ApJ, 538, 793
Krist, J. E., Stapelfeldt, K. R., & Watson, A. M. 2002, ApJ, 570, 785
Krist, J. E., et al. 1998, ApJ, 501, 841
———. 2005, AJ, 130, 2778
Kuhn, J. R., Potter, D., & Parise, B. 2001, ApJ, 553, L 189
Kuiper, G. P. 1956, JRASC, 50, 158
Kusaka, T., Nakano, T., & Hayashi, C. 1970, Prog. Theor. Phys., 44, 1580
Kusakabe, N., et al. 2012, ApJ, 753, 153
Lada, C. J. 1985, ARA&A, 23, 267
Lada, C. J., & Lada, E. A. 2003, ARA&A, 41, 57
Lada, C. J., & Wilking, B. A. 1984, ApJ, 287, 610
Laor, A., & Draine, B. T. 1993, ApJ, 402, 441
Laplace, P. S. 1796, Exposition du Systéme du Monde
Larson, R. B. 1969, MNRAS, 145, 271
Larson, R. B. 1972, MNRAS, 157, 121
Larwood, J. D. 1997, MNRAS, 290, 490
Laughlin, G., Bodenheimer, P., & Adams, F. C. 2004, ApJ, 612, L 73
Lay, O. P., Carlstrom, J. E., & Hills, R. E. 1997, ApJ, 489, 917
Lay, O. P., Carlstrom, J. E., Hills, R. E., & Phillips, T. G. 1994, ApJ, 434, L 75
Lazareff, B., Monin, J.-L., & Pudritz, R. E. 1990, ApJ, 358, 170
Lee, N., Williams, J. P., & Cieza, L. A. 2011, ApJ, 736, 135
Leinert, Ch., Zinnecker, H., Weitzel, N., Christou, J., Ridgway, S. T., Jameson, R., Haas, M., & Lenzen, R. 1993, A&A, 278, 129
Li, A., & Draine, B. T. 2001, ApJ, 554, 778
Liffman, K. 2003, Proc. Astron. Soc. Australia, 20, 337
Lin, D. N. C., Faulkner, J., & Papaloizou, J. 1985, MNRAS, 212, 105
Lin, D. N. C., & Papaloizou, J. 1979, MNRAS, 186, 799
———. 1980, MNRAS, 191, 37
———. 1985, in Protostars and Planets II, ed. D. C. Black, & M. S. Matthews (Tucson: Univ. Arizona Press), 981
Lin, D. N. C., & Papaloizou, J. C. B. 1993, in Protostars and Planets III, ed. E. H. Levy, & J. I. Lunine (Tucson: Univ. Arizona Press), 749
Lin, D. N. C., & Pringle, J. E. 1987, MNRAS, 225, 607
Lissauer, J. J. 1993, ARA&A, 31, 129
Lodders, K. 2003, ApJ, 591, 1220
Lommen, D., Maddison, S. T., Wright, C. M., van Dishoeck, E. F., Wilner, D. J., & Bourke, T. L. 2009, A&A, 495, 869
Lommen, D., et al. 2007, A&A, 462, 211
Lommen, D. J. P., et al. 2010, A&A, 515, A 77
Looney, L. W., Mundy, L. G., & Welch, W. J. 2000, ApJ, 529, 477
Lubow, S. H., & D'Angelo, G. 2006, ApJ, 641, 526
Lubow, S. H., Seibert, M., & Artymowicz, P. 1999, ApJ, 526, 1001
Lucas, P. W., & Roche, P. F. 1997, MNRAS, 286, 895
Lucy, L. B. 1999, A&A, 344, 282
Lynden-Bell, D., & Pringle, J. E. 1974, MNRAS, 168, 603
Lyra, W., & Lin, M.-K. 2013, ApJ, 775, 17
Malbet, F., & Bertout, C. 1991, ApJ, 383, 814
Malbet, F., Lachaume, R., & Monin, J.-L. 2001, A&A, 379, 515
Mamajek, E. E. 2009, in AIP Conf. Ser. 1158, Exoplanets and Disks: Their Formation and Diversity, ed. T. Usuda, Tamura, M., & Ishii, M. (Melville: AIP), 3
Manara, C. F., Testi, L., Natta, A., Rosotti, G., Benisty, M., Ercolano, B., & Ricci, L. 2014, A&A, 568, A 18
Mann, R. K., & Williams, J. P. 2009, ApJ, 694, L 36
———. 2010, ApJ, 725, 430

Mann, R. K., et al. 2014, ApJ, 784, 82
———. 2015, ApJ, 802, 77
Mannings, V., & Emerson, J. P. 1994, MNRAS, 267, 361
Mannings, V., & Sargent, A. I. 1997, ApJ, 490, 792
Marcy, G., Butler, R. P., Fischer, D., Vogt, S., Wright, J. T., Tinney, C. G., & Jones, H. R. A. 2005, Prog. Theor. Phys. Suppl., 158, 24
Marino, S., Perez, S., & Casassus, S. 2015, ApJ, 798, L 44
Marsh, K. A., & Mahoney, M. J. 1992, ApJ, 395, L 115
———. 1993, ApJ, 405, L 71
Marzari, F., Scholl, H., Thébault, P., & Baruteau, C. 2009, A&A, 508, 1493
Mathews, G. S., Williams, J. P., Ménard, F., Phillips, N., Duchêne, G., & Pinte, C. 2012, ApJ, 745, 23
Mathews, G. S., et al. 2013, A&A, 557, A 132
Mathis, J. S. 1990, ARA&A, 28, 37
Mathis, J. S., Rumpl, W., & Nordsieck, K. H. 1977, ApJ, 217, 425
Matsuyama, I., Johnstone, D., & Murray, N. 2003, ApJ, 585, L 143
McCabe, C., Duchêne, G., Pinte, C., Stapelfeldt, K. R., Ghez, A. M., & Ménard, F. 2011, ApJ, 727, 90
McCabe, C., Ghez, A. M., Prato, L., Duchêne, G., Fisher, R. S., & Telesco, C. 2006, ApJ, 636, 932
McCaughrean, M. J., & O'dell, C. R. 1996, AJ, 111, 1977
McCaughrean, M. J., Stapelfeldt, K. R., & Close, L. M. 2000, in Protostars and Planets IV, ed. V. Mannings, A. P. Boss, & S. S. Russell (Tucson: Univ. Arizona Press), 485
McClure, M. K., et al. 2015, ApJ, 799, 162
Meeus, G., Sterzik, M., Bouwman, J., & Natta, A. 2003, A&A, 409, L 25
Meeus, G., Waters, L. B. F. M., Bouwman, J., van den Ancker, M. E., Waelkens, C., & Malfait, K. 2001, A&A, 365, 476
Mendoza, V., & Eugenio, E. 1966, ApJ, 143, 1010
———. 1968, ApJ, 151, 977
Menu, J., et al. 2014, A&A, 564, A 93
Merín, B., et al. 2010, ApJ, 718, 1200
Miguel, Y., Guilera, O. M., & Brunini, A. 2011, MNRAS, 412, 2113
Millan-Gabet, R., Malbet, F., Akeson, R., Leinert, C., Monnier, J., & Waters, R. 2007, in Protostars and Planets V, ed. B. Reipurth, D. Jewitt, & K. Keil (Tucson: Univ. Arizona Press), 539
Min, M., Canovas, H., Mulders, G. D., & Keller, C. U. 2012, A&A, 537, A 75
Min, M., Dominik, C., & Waters, L. B. F. M. 2004, A&A, 413, L 35
Min, M., Dullemond, C. P., Dominik, C., de Koter, A., & Hovenier, J. W. 2009, A&A, 497, 155
Min, M., Hovenier, J. W., & de Koter, A. 2003, A&A, 404, 35
———. 2005, A&A, 432, 909
Mittal, T., & Chiang, E. 2015, ApJ, 798, L 25
Miyake, K., & Nakagawa, Y. 1993, Icarus, 106, 20
———. 1995, ApJ, 441, 361
Mizuno, H. 1980, Prog. Theor. Phys., 64, 544
Mohanty, S., et al. 2013, ApJ, 773, 168
Morales-Calderón, M., et al. 2009, ApJ, 702, 1507
Motte, F., Andre, P., & Neri, R. 1998, A&A, 336, 150
Moulton, F. R. 1900, ApJ, 11, 103
———. 1905, ApJ, 22, 165
Mulders, G. D., & Dominik, C. 2012, A&A, 539, A 9
Mulders, G. D., Min, M., Dominik, C., Debes, J. H., & Schneider, G. 2013, A&A, 549, A 112
Mundy, L. G., Looney, L. W., & Lada, E. A. 1995, ApJ, 452, L 137
Mundy, L. G., et al. 1996, ApJ, 464, L 169
Muto, T., et al. 2012, ApJ, 748, L 22
Muzerolle, J., Allen, L. E., Megeath, S. T., Hernández, J., & Gutermuth, R. A. 2010, ApJ, 708, 1107
Muzerolle, J., Luhman, K. L., Briceño, C., Hartmann, L., & Calvet, N. 2005, ApJ, 625, 906
Muzerolle, J., et al. 2009, ApJ, 704, L 15
Najita, J. R., Andrews, S. M., & Muzerolle, J. 2015, MNRAS, 378, 369
Najita, J. R., & Kenyon, S. J. 2014, MNRAS, 445, 3315
Najita, J. R., Strom, S. E., & Muzerolle, J. 2007, MNRAS, 378, 369
Nakagawa, Y., Nakazawa, K., & Hayashi, C. 1981, Icarus, 45, 517
Nakagawa, Y., Sekiya, M., & Hayashi, C. 1986, Icarus, 67, 375
Narayanan, D., Kulesa, C. A., Boss, A., & Walker, C. K. 2006, ApJ, 647, 1426
Natta, A., Prusti, T., Neri, R., Wooden, D., Grinin, V. P., & Mannings, V. 2001, A&A, 371, 186
Natta, A., Testi, L., Calvet, N., Henning, T., Waters, R., & Wilner, D. 2007, in Protostars and Planets V, ed. V. Mannings, A. P. Boss, & S. S. Russell (Tucson: Univ. Arizona Press), 767
Natta, A., Testi, L., Neri, R., Shepherd, D. S., & Wilner, D. J. 2004, A&A, 416, 179
Natta, A., Testi, L., & Randich, S. 2006, A&A, 452, 245
Nuernberger, D., Brandner, W., Yorke, H. W., & Zinnecker, H. 1998, A&A, 330, 549
Nuernberger, D., Chini, R., & Zinnecker, H. 1997, A&A, 324, 1036
Öberg, K. I., et al. 2010, ApJ, 720, 480
———. 2011, ApJ, 734, 98
Ochi, Y., Sugimoto, K., & Hanawa, T. 2005, ApJ, 623, 922
O'dell, C. R., & Wen, Z. 1994, ApJ, 436, 194
O'dell, C. R., Wen, Z., & Hu, X. 1993, ApJ, 410, 696
Okuzumi, S. 2009, ApJ, 698, 1122
Okuzumi, S., Tanaka, H., Kobayashi, H., & Wada, K. 2012, ApJ, 752, 106
Oliveira, I., Olofsson, J., Pontoppidan, K. M., van Dishoeck, E. F., Augereau, J.-C., & Merín, B. 2011, ApJ, 734, 51
Oliveira, I., et al. 2010, ApJ, 714, 778
Olofsson, J., et al. 2009, A&A, 507, 327
Ormel, C. W., Min, M., Tielens, A. G. G. M., Dominik, C., & Paszun, D. 2011, A&A, 532, A 43
Ormel, C. W., Spaans, M., & Tielens, A. G. G. M. 2007, A&A, 461, 215
Osorio, M., et al. 2014, ApJ, 791, L 36
Ossenkopf, V. 1993, A&A, 280, 617
Ossenkopf, V., & Henning, T. 1994, A&A, 291, 943
Osterloh, M., & Beckwith, S. V. W. 1995, ApJ, 439, 288
Owen, J. E., & Clarke, C. J. 2012, MNRAS, 426, L 96
Owen, J. E., Clarke, C. J., & Ercolano, B. 2012, MNRAS, 422, 1880
Owen, J. E., Ercolano, B., & Clarke, C. J. 2011, MNRAS, 412, 13
Owen, J. E., Ercolano, B., Clarke, C. J., & Alexander, R. D. 2010, MNRAS, 401, 1415
Owen, J. E., Hudoba de Badyn, M., Clarke, C. J., & Robins, L. 2013, MNRAS, 436, 1430
Paardekooper, S.-J., & Mellema, G. 2006, A&A, 453, 1129
Paardekooper, S.-J., Thébault, P., & Mellema, G. 2008, MNRAS, 386, 973
Padgett, D. L., Brandner, W., Stapelfeldt, K. R., Strom, S. E., Tereby, S., & Koerner, D. 1999, AJ, 117, 1490

Panić, O., Hogerheijde, M. R., Wilner, D., & Qi, C. 2009, A&A, 501, 269
Papaloizou, J. C. B., & Lin, D. N. C. 1995, ARA&A, 33, 505
Pascucci, I., Apai, D., Hardegree-Ullman, E. E., Kim, J. S., Meyer, M. R., & Bouwman, J. 2008, ApJ, 673, 477
Patience, J., Akeson, R. L., & Jensen, E. L. N. 2008, ApJ, 677, 616
Patience, J., et al. 2002, ApJ, 581, 654
Pérez, L. M., Isella, A., Carpenter, J. M., & Chandler, C. J. 2014, ApJ, 783, L 13
———. 2015, ApJ, 783, L 13
Pérez, L. M., et al. 2012, ApJ, 760, L 17
———. 2015, ApJ, 798, 85
Perrin, M. D., Duchêne, G., Kalas, P., & Graham, J. R. 2006, ApJ, 645, 1272
Perrin, M. D., Graham, J. R., Kalas, P., Lloyd, J. P., Max, C. E., Gavel, D. T., Pennington, D. M., & Gates, E. L. 2004, Science, 303, 1345
Perrin, M. D., et al. 2015, ApJ, 799, 182
Pfalzner, S., Steinhausen, M., & Menten, K. 2014, ApJ, 793, L 34
Piétu, V., Dutrey, A., Guilloteau, S., Chapillon, E., & Pety, J. 2006, A&A, 460, L 43
Piétu, V., Guilloteau, S., Di Folco, E., Dutrey, A., & Boehler, Y. 2014, A&A, 564, A 95
Piétu, V., Guilloteau, S., & Dutrey, A. 2005, A&A, 443, 945
Pinilla, P., Benisty, M., & Birnstiel, T. 2012a, A&A, 545, A 81
———. 2015, A&A, 545, A 81
Pinilla, P., Birnstiel, T., Ricci, L., Dullemond, C. P., Uribe, A. L., Testi, L., & Natta, A. 2012b, A&A, 538, A 114
Pinte, C., Fouchet, L., Ménard, F., Gonzalez, J.-F., & Duchêne, G. 2007, A&A, 469, 963
Pinte, C., Ménard, F., Duchêne, G., & Bastien, P. 2006, A&A, 459, 797
Pinte, C., et al. 2008, A&A, 489, 633
Pollack, J. B., Hollenbach, D., Beckwith, S., Simonelli, D. P., Roush, T., & Fong, W. 1994, ApJ, 421, 615
Pollack, J. B., Hubickyj, O., Bodenheimer, P., Lissauer, J. J., Podolak, M., & Greenzweig, Y. 1996, Icarus, 124, 62
Porras, A., Christopher, M., Allen, L., Di Francesco, J., Megeath, S. T., & Myers, P. C. 2003, AJ, 126, 1916
Pott, J.-U., Perrin, M. D., Furlan, E., Ghez, A. M., Herbst, T. M., & Metchev, S. 2010, ApJ, 710, 265
Potter, D. E., Close, L. M., Roddier, F., Roddier, C., Graves, J. E., & Northcott, M. 2000, ApJ, 540, 422
Pringle, J. E. 1981, ARA&A, 19, 137
Proszkow, E.-M., & Adams, F. C. 2009, ApJS, 185, 486
Purcell, E. M., & Pennypacker, C. R. 1973, ApJ, 186, 705
Qi, C., D'Alessio, P., Öberg, K. I., Wilner, D. J., Hughes, A. M., Andrews, S. M., & Ayala, S. 2011, ApJ, 740, 84
Qi, C., et al. 2013, Science, 341, 630
Quanz, S. P., Amara, A., Meyer, M. R., Girard, J. H., Kenworthy, M. A., & Markus, K. 2015, ApJ, 807, 64
Quanz, S. P., Schmid, H. M., Geissler, K., Meyer, M. R., Henning, T., Brandner, W., & Wolf, S. 2011, ApJ, 738, 23
Quillen, A. C. 2006, ApJ, 640, 1078
Raghavan, D., Henry, T. J., Mason, B. D., Subasavage, J. P., Jao, W.-C., Beaulieu, T. D., & Hambly, N. C. 2006, ApJ, 646, 523
Raghavan, D., et al. 2010, ApJS, 190, 1
Rapson, V. A., Kastner, J. H., Andrews, S. M., Hines, D. C., Macintosh, B., Millar-Blanchaer, M., & Tamura, M. 2015, ApJ, 803, L 10
Raymond, S. N., Quinn, T., & Lunine, J. I. 2004, Icarus, 168, 1
———. 2005, ApJ, 632, 670
Rebull, L. M., et al. 2014, AJ, 148, 92
Regály, Z., Juhász, A., Sándor, Z., & Dullemond, C. P. 2012, MNRAS, 419, 1701
Reggiani, M., et al. 2014, ApJ, 792, L 23
Reipurth, B., Clarke, C. J., Boss, A. P., Goodwin, S. P., Rodríguez, L. F., Stassun, K. G., Tokovinin, A., & Zinnecker, H. 2014, in Protostars and Planets VI, ed. H. Beuther, et al. (Tucson: Univ. Arizona Press), 267
Reipurth, B., & Zinnecker, H. 1993, A&A, 278, 81
Ricci, L., Testi, L., Natta, A., & Brooks, K. J. 2010a, A&A, 521, A 66
Ricci, L., Testi, L., Natta, A., Neri, R., Cabrit, S., & Herczeg, G. J. 2010b, A&A, 512, A 15
Ricci, L., Trotta, F., Testi, L., Natta, A., Isella, A., & Wilner, D. J. 2012, A&A, 540, A 6
Rice, W. K. M., Armitage, P. J., Wood, K., & Lodato, G. 2006, MNRAS, 373, 1619
Rice, W. K. M., Wood, K., Armitage, P. J., Whitney, B. A., & Bjorkman, J. E. 2003, MNRAS, 342, 79
Robberto, M., et al. 2013, ApJS, 207, 10
Roberge, A., Weinberger, A. J., & Malumuth, E. M. 2005, ApJ, 622, 1171
Robitaille, T. P. 2011, A&A, 536, A 79
Robitaille, T. P., Whitney, B. A., Indebetouw, R., Wood, K., & Denzmore, P. 2006, ApJS, 167, 256
Roddier, C., Roddier, F., Northcott, M. J., Graves, J. E., & Jim, K. 1996, ApJ, 463, 326
Rodigas, T. J., et al. 2015, ApJ, 798, 96
Rodmann, J., Henning, T., Chandler, C. J., Mundy, L. G., & Wilner, D. J. 2006, A&A, 446, 211
Rosenfeld, K. A., Andrews, S. M., Hughes, A. M., Wilner, D. J., & Qi, C. 2013a, ApJ, 774, 16
Rosenfeld, K. A., Andrews, S. M., Wilner, D. J., Kastner, J. H., & McClure, M. K. 2013b, ApJ, 775, 136
Rosenfeld, K. A., Chiang, E., & Andrews, S. M. 2014, ApJ, 782, 62
Rosenfeld, K. A., et al. 2012, ApJ, 757, 129
Rosotti, G. P., Ercolano, B., Owen, J. E., & Armitage, P. J. 2013, MNRAS, 430, 1392
Rucinski, S. M. 1985, AJ, 90, 2321
Ruden, S. P., & Lin, D. N. C. 1986, ApJ, 308, 883
Ruden, S. P., & Pollack, J. B. 1991, ApJ, 375, 740
Rybicki, G. B., & Lightman, A. P. 1979, Radiative Processes in Astrophysics (New York: Wiley), chap. 1
Rydgren, A. E. 1984, Publ. US Naval Obs. 2nd Ser., 25, 1
Rydgren, A. E., Schmelz, J. T., & Vrba, F. J. 1982, ApJ, 256, 168
Rydgren, A. E., Strom, S. E., & Strom, K. M. 1976, ApJS, 30, 307
Rydgren, A. E., & Vrba, F. J. 1981, AJ, 86, 1069
———. 1983, AJ, 88, 1017
Rydgren, A. E., & Zak, D. S. 1987, PASP, 99, 141
Salyk, C., Blake, G. A., Boogert, A. C. A., & Brown, J. M. 2009, ApJ, 699, 330
Sargent, A. I., & Beckwith, S. 1987, ApJ, 323, 294
Sargent, A. I., & Beckwith, S. V. W. 1991, ApJ, 382, L 31
Sargent, B., et al. 2006, ApJ, 645, 395
Sargent, B. A., et al. 2009a, ApJS, 182, 477
Sargent, B. A., et al. 2009b, ApJ, 690, 1193

Schaefer, G. H., Dutrey, A., Guilloteau, S., Simon, M., & White, R. J. 2009, ApJ, 701, 698
Schneider, G., Wood, K., Silverstone, M. D., Hines, D. C., Koerner, D. W., Whitney, B. A., Bjorkman, J. E., & Lowrance, P. J. 2003, AJ, 125, 1467
Scholz, A., Jayawardhana, R., & Wood, K. 2006, ApJ, 645, 1498
Schräpler, R., & Henning, T. 2004, ApJ, 614, 960
Seizinger, A., Krijt, S., & Kley, W. 2013, A&A, 560, A 45
Shakura, N. I., & Sunyaev, R. A. 1973, A&A, 24, 337
Shu, F. H., Adams, F. C., & Lizano, S. 1987, ARA&A, 25, 23
Sicilia-Aguilar, A., Hartmann, L. W., Hernández, J., Briceño, C., & Calvet, N. 2005, AJ, 130, 188
Sicilia-Aguilar, A., Henning, T., & Hartmann, L. W. 2010, ApJ, 710, 597
Sicilia-Aguilar, A., Henning, T., Juhász, A., Bouwman, J., Garmire, G., & Garmire, A. 2008, ApJ, 687, 1145
Siess, L., Dufour, E., & Forestini, M. 2000, A&A, 358, 593
Simon, M., et al. 1995, ApJ, 443, 625
Sitko, M. L., et al. 2008, ApJ, 678, 1070
Skrutskie, M. F., Dutkevitch, D., Strom, S. E., Edwards, S., Strom, K. M., & Shure, M. A. 1990, AJ, 99, 1187
Smith, N., Bally, J., & Morse, J. A. 2003, ApJ, 587, L 105
Soderblom, D. R., Hillenbrand, L. A., Jeffries, R. D., Mamajek, E. E., & Naylor, T. 2014, in Protostars and Planets VI, ed. H. Beuther, et al. (Tucson: Univ. Arizona Press), 219
Stapelfeldt, K. R., Krist, J. E., Ménard, F., Bouvier, J., Padget, D. L., & Burrows, C. J. 1998, ApJ, 502, L 65
Stapelfeldt, K. R., Ménard, F., Watson, A. M., Krist, J. E., Dougados, C., Padgett, D. L., & Brandner, W. 2003, ApJ, 589, 410
Stapelfeldt, K. R., et al. 1999, ApJ, 516, L 95
Stepinski, T. F. 1998, Icarus, 132, 100
Strom, K. M., Strom, S. E., Edwards, S., Cabrit, S., & Skrutskie, M. F. 1989, AJ, 97, 1451
Strom, K. M., Strom, S. E., Kenyon, S. J., & Hartmann, L. 1988, AJ, 95, 534
Strom, K. M., Strom, S. E., & Yost, J. 1971, ApJ, 165, 479
Strom, S. E. 1972, PASP, 84, 745
Strom, S. E., Strom, K. M., Brooke, A. L., Bregman, J., & Yost, J. 1972, ApJ, 171, 267
Strom, S. E., Strom, K. M., & Grasdalen, G. L. 1975, ARA&A, 13, 187
Strom, S. E., Strom, K. M., Grasdalen, G. L., Capps, R. W., & Thompson, D. 1985, AJ, 90, 2575
Sturm, B., et al. 2013, A&A, 553, A 5
Suzuki, T. K., & Inutsuka, S.-i. 2014, ApJ, 784, 121
Takami, M., et al. 2014, ApJ, 795, 71
Takeuchi, T., Clarke, C. J., & Lin, D. N. C. 2005, ApJ, 627, 286
Takeuchi, T., & Lin, D. N. C. 2002, ApJ, 581, 1344
———. 2005, ApJ, 623, 482
Tamura, M., SEEDS Team 2009, in AIP Conf. Ser. 1158, Exoplanets and Disks: Their Formation and Diversity, ed. T. Usuda, M. Tamura, & M. Ishii (Melville: AIP), 11
Terebey, S., Shu, F. H., & Cassen, P. 1984, ApJ, 286, 529
Testi, L., Natta, A., Shepherd, D. S., & Wilner, D. J. 2003, A&A, 403, 323
Testi, L., et al. 2014, in Protostars and Planets VI, ed. H. Beuther, et al. (Tucson: Univ. Arizona Press), 339
Thamm, E., Steinacker, J., & Henning, T. 1994, A&A, 287, 493
Trilling, D. E., Koerner, D. W., Barnes, J. W., Ftaclas, C., & Brown, R. H. 2001, ApJ, 552, L 151
Trotta, F., Testi, L., Natta, A., Isella, A., & Ricci, L. 2013, A&A, 558, A 64
Tsukagoshi, T., et al. 2014, ApJ, 783, 90
Turner, N. J., Fromang, S., Gammie, C., Klahr, H., Lesur, G., Wardle, M., & Bai, X. N. 2014, in Protostars and Planets VI, ed. H. Beuther, et al. (Tucson: Univ. Arizona Press), 411
Ubach, C., Maddison, S. T., Wright, C. M., Wilner, D. J., Lommen, D. J. P., & Koribalski, B. 2012, MNRAS, 425, 3137
Uchida, Y., & Shibata, K. 1984, PASJ, 36, 105
Udry, S., & Santos, N. C. 2007, ARA&A, 45, 397
van der Marel, N., van Dishoeck, E., Bruderer, S., Perez, L. M., & Isella, A. 2015, A&A, 579, 176
van der Marel, N., et al. 2013, Science, 340, 1199
Varnière, P., Blackman, E. G., Frank, A., & Quillen, A. C. 2006, ApJ, 640, 1110
Verrier, P. E., & Evans, N. W. 2008, MNRAS, 390, 1377
Völk, H. J., Jones, F. C., Morfill, G. E., & Roeser, S. 1980, A&A, 85, 316
Vrba, F. J., Schmidt, G. D., & Hintzen, P. M. 1979, ApJ, 227, 185
Wada, K., Tanaka, H., Suyama, T., Kimura, H., & Yamamoto, T. 2009, ApJ, 702, 1490
Waelkens, C., et al. 1996, A&A, 315, L 245
Walsh, C., et al. 2014, ApJ, 791, L 6
Wang, J., Xie, J.-W., Barclay, T., & Fischer, D. A. 2014, ApJ, 783, 4
Warner, J. W., Strom, S. E., & Strom, K. M. 1977, ApJ, 213, 427
Watson, A. M., & Stapelfeldt, K. R. 2004, ApJ, 602, 860
———. 2007, AJ, 133, 845
Watson, A. M., Stapelfeldt, K. R., Wood, K., & Ménard, F. 2007, in Protostars and Planets V, ed. B. Reipurth, D. Jewitt, & K. Keil (Tucson: Univ. Arizona Press), 523
Watson, D. M., et al. 2009, ApJS, 180, 84
Weidenschilling, S. J. 1977a, MNRAS, 180, 57
———. 1977b, Ap&SS, 51, 153
———. 2003, Icarus, 165, 438
Weintraub, D. A., Sandell, G., & Duncan, W. D. 1989, ApJ, 340, L 69
Whipple, F. L. 1972, in From Plasma to Planet, ed. A. Elvius (New York: Wiley), 211
White, R. J., & Ghez, A. M. 2001, ApJ, 556, 265
Whitney, B. A., & Hartmann, L. 1992, ApJ, 395, 529
Whitney, B. A., Wood, K., Bjorkman, J. E., & Cohen, M. 2003, ApJ, 598, 1079
Wilking, B. A., Lada, C. J., & Young, E. T. 1989, ApJ, 340, 823
Williams, J. P., Andrews, S. M., & Wilner, D. J. 2005, ApJ, 634, 495
Williams, J. P., & Best, W. M. J. 2014, ApJ, 788, 59
Williams, J. P., & Cieza, L. A. 2011, ARA&A, 49, 67
Williams, J. P., et al. 2013, MNRAS, 435, 1671
———. 2014, ApJ, 796, 120
Wilner, D. J., Bourke, T. L., Wright, C. M., Jørgensen, J. K., van Dishoeck, E. F., & Wong, T. 2003, ApJ, 596, 597
Wilner, D. J., D'Alessio, P., Calvet, N., Claussen, M. J., & Hartmann, L. 2005, ApJ, 626, L 109
Wilner, D. J., Ho, P. T. P., Kastner, J. H., & Rodrguez, L. F. 2000, ApJ, 534, L 101
Wilner, D. J., Ho, P. T. P., & Rodriguez, L. F. 1996, ApJ, 470, L 117

Wilner, D. J., & Lay, O. P. 2000, in Protostars and Planets IV, ed. V. Mannings, A. P. Boss, & S. S. Russell (Tucson: Univ. Arizona Press), 509
Winn, J. N., & Fabrycky, D. C. 2015, ARA&A, 53, 409
Wisniewski, J. P., Clampin, M., Grady, C. A., Ardila, D. R., Ford, H. C., Golimowski, D. A., Illingworth, G. D., & Krist, J. E. 2008, ApJ, 682, 548
Wolf, S., Henning, T., & Stecklum, B. 1999, A&A, 349, 839
Wolf, S., & Klahr, H. 2002, ApJ, 578, L 79
Wolf, S., Padgett, D. L., & Stapelfeldt, K. R. 2003, ApJ, 588, 373
Wood, J. A., & Morfill, G. E. 1988, in Meteorites and the Early Solar System, ed. J. F. Kerridge, & M. S. Matthews (Tucson, Univ. Arizona Press), 329
Wood, K., Kenyon, S. J., Whitney, B., & Turnbull, M. 1998, ApJ, 497, 404
Youdin, A. N., & Shu, F. H. 2002, ApJ, 580, 494
Young, A. S. 1901, ApJ, 13, 338
Zhang, K., Isella, A., Carpenter, J. M., & Blake, G. A. 2014, ApJ, 791, 42
Zhu, Z., Nelson, R. P., Dong, R., Espaillat, C., & Hartmann, L. 2012, ApJ, 755, 6
Zhu, Z., Nelson, R. P., Hartmann, L., Espaillat, C., & Calvet, N. 2011, ApJ, 729, 47
Zhu, Z., & Stone, J. M. 2014, ApJ, 795, 53
Zhu, Z., Stone, J. M., Rafikov, R. R., & Bai, X.-n. 2014, ApJ, 785, 122
Zsom, A., Ormel, C. W., Güttler, C., Blum, J., & Dullemond, C. P. 2010, A&A, 513, A 57
Zubko, V. G., Mennella, V., Colangeli, L., & Bussoletti, E. 1996, MNRAS, 282, 1321